AUGUST 1966
REPORT SM-48464-TPR-3

RESEARCH ON THE UTILIZATION OF PATTERN RECOGNITION TECHNIQUES TO IDENTIFY AND CLASSIFY OBJECTS IN VIDEO DATA

TECHNICAL PROGRESS REPORT NO. 3
COVERING PERIOD FROM
20 MAY 1966 THROUGH 29 JULY 1966

PREPARED UNDER CONTRACT NAS 12-30
FOR THE
NATIONAL AERONAUTICS & SPACE ADMINISTRATION
ELECTRONICS RESEARCH CENTER
CAMBRIDGE, MASSACHUSETTS

ASTROPOWER LABORATORY
2121 CAMPUS DRIVE • NEWPORT BEACH, CALIFORNIA

MISSILE & SPACE SYSTEMS DIVISION
DOUGLAS AIRCRAFT COMPANY, INC.
SANTA MONICA CALIFORNIA

DOUGLAS

Report SM-48464-TPR-3

RESEARCH ON THE UTILIZATION OF PATTERN RECOGNITION TECHNIQUES TO IDENTIFY AND CLASSIFY OBJECTS IN VIDEO DATA

Technical Progress Report No. 3
Covering Period From
20 May 1966 Through 29 July 1966

Prepared Under Contract NAS 12-30
for the
National Aeronautics and Space Administration
Electronics Research Center
Cambridge, Massachusetts

MISSILE & SPACE SYSTEMS DIVISION
ASTROPOWER LABORATORY
Douglas Aircraft Company, Inc.
Newport Beach, California

FOREWORD

This report was prepared by the Astropower Laboratory of the Douglas Aircraft Company, Inc., Newport Beach, California, in fulfillment of NASA contract NAS 12-30. The work was sponsored by the NASA Electronics Research Center, Cambridge, Massachusetts. Mr. Eugene M. Darling, Jr. was the Technical Officer for this offfice.

The studies began on June 18, 1965. This document is the third technical report.

Work on the contract was performed by the Electronics Department of the Astropower Laboratory. The contributors were G. E. Axtelle, R. D. Joseph, C. C. Kesler, W. B. Martin, J. N. Medick, A. G. Ostensoe, R. G. Runge, and S. S. Viglione.

SUMMARY

This report covers the Item 2 NIMBUS cloud pattern experiments and the Item 3 spaceborne recognition processor feasibility studies called for under contract NAS 12-30.

The NIMBUS experiments lead to the conclusion that two of the pattern recognition system design techniques appear to have significant advantages over the other 10 studied. The best techniques achieved performance levels of about 90%. Although higher performance is desirable for an operational system, the levels achieved are compatible with the number and quality of the sample patterns used, and the minimal extent of the preprocessing considered.

The feasibility of two parallel/analog implementations of a spaceborne recognition processor was investigated in detail. Although operationally feasible, both systems suffer from the requirement for excessive power and weight as a result of the restriction to consider off-the-shelf components only. Serial/digital approaches are suggested, but were not studied in detail. These latter approaches will not present weight or power difficulties, but need to be studied to determine whether or not processing time is commensurate with the parallel analog configurations.

TABLE OF CONTENTS

LIST OF ILLUSTRATIONS

LIST OF TABLES

1.0 INTRODUCTION

1.1 Purpose and Scope of the Program

The number of adaptive techniques for the design of pattern recognition networks has been proliferating. Comparisons of these techniques, however, are virtually nonexistent. Therefore, the principal objective of the pattern recognition experiments conducted under this contract was to determine the comparative performance of several state-of-the-art techniques on two recognition problems. These techniques are the ones which a literature survey (Technical Report No. 1) revealed to be both frequently reported and promising.

Two recognition problems were considered. The first entailed discrimination among four classes of lunar topographic features; the second involved the classification of three NIMBUS cloud patterns. The lunar experiments are described in Technical Report No. 2. Based on these results six techniques were discarded and six retained for the experiments on the NIMBUS patterns. The results of the experiments on the NIMBUS data are presented in this report.

The feasibility of constructing a spaceborne recognition processor with off-the-shelf hardware was examined. A detailed study of two parallel/analog systems is reported. Also a promising serial/digital implementation is suggested. This approach will be explored during the next reporting period.

2.0 GENERATION OF NIMBUS CLOUD PATTERN FILES

2.1 Origin of Pattern Sets

For the second phase of this program pattern recognition experiments were based on a set of photographic reproductions of video cloud patterns transmitted from the NIMBUS I satellite. Mr. Eugene M. Darling, Jr., NASA Technical Officer, examined numerous photographs and selected 323 examples of the three desired classifications from 311 picture frames. The cloud patterns are categorized in Table I.

TABLE I

CLOUD PATTERN CATEGORIES

Feature	Training Set (No. of Examples)	Generalization Set (No. of Examples)
Noncumulus	80	28
Cumulus, Polygonal Cells	80	16
Cumulus, Solid Cells	80	39

Mr. Darling also provided a subjective judgment of how well each frame depicts the pattern in question using this scale:

G, Good – These are the best cases showing the pattern in its most typical form.

F, Fair – The pattern shown is acceptable, but departs to a greater or lesser degree from its typical form.

P, Poor – The pattern is barely identifiable. These cases are of marginal use.

The distribution of pattern class with respect to pattern quality is shown in Table II.

In addition Mr. Darling describes the patterns as follows:

"The two cumulus patterns are characterized by cellular elements. Polygonal cells consist of a wall of cloud surrounding a clear area. In some cases this wall completely encloses the central clear region; in others the wall is open and the pattern becomes vermiculated (i. e., worm-like). For the purposes of this study both the open and the

TABLE II

PATTERN QUALITY

Pattern Quality	Pattern Class (Number of Cases)		
	Noncumulus	Cumulus Polygonal Cells	Cumulus Solid Cells
Good	53	59	65
Fair	47	37	50
Poor	8	0	4

closed walls are lumped together into a single pattern called polygonal cells." (See Figure 1.)

"The solid cell case is (as the name implies) an unbroken mass of cloud, very bright, with sharp edges surrounded by a clear boundary. The solid cell may stand isolated from other clouds by a distinct expanse of clear air or may be embedded in a densely packed assemblage of cells where the boundary between cells is barely visible." (See Figure 2.)

"Noncumulus clouds appear typically in fibrous, diffuse sheets on filaments without distinct edges and without a cellular structure." (See Figure 3.)

"It is important to understand that a 'pattern' in the context of these experiments is not a single cell, but rather is an assemblage of many (or at least several) cells. The pattern must also be chosen to include a large fraction of cloud — at least 60% or so."

2.2 Pattern Processing

The processing of the patterns selected for this program involved converting the photographic patterns to video patterns using a slow scan television system. The video output of the TV system was recorded to allow batch analog-to-digital conversion of the video patterns. After analog-to-digital conversion at a sampling rate consistent with the resolution desired, the digital tapes produced were processed by a computer program which isolated the pictures and adjusted gray scale levels to compensate for changes in video gain in the TV system. This program also reduced the resolution of the pictures and stored the patterns in a standardized formation on digital magnetic tapes. The resolution was reduced by summing the gray scale values

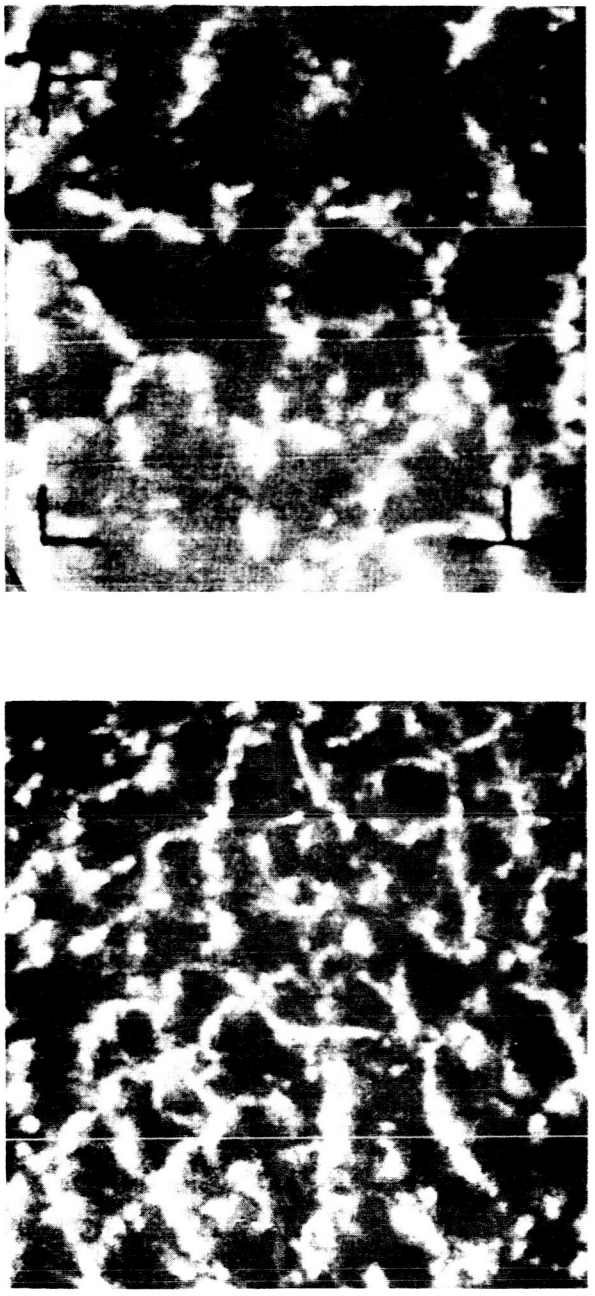

c1009

Figure 1. Cumulus, Polygonal Cells

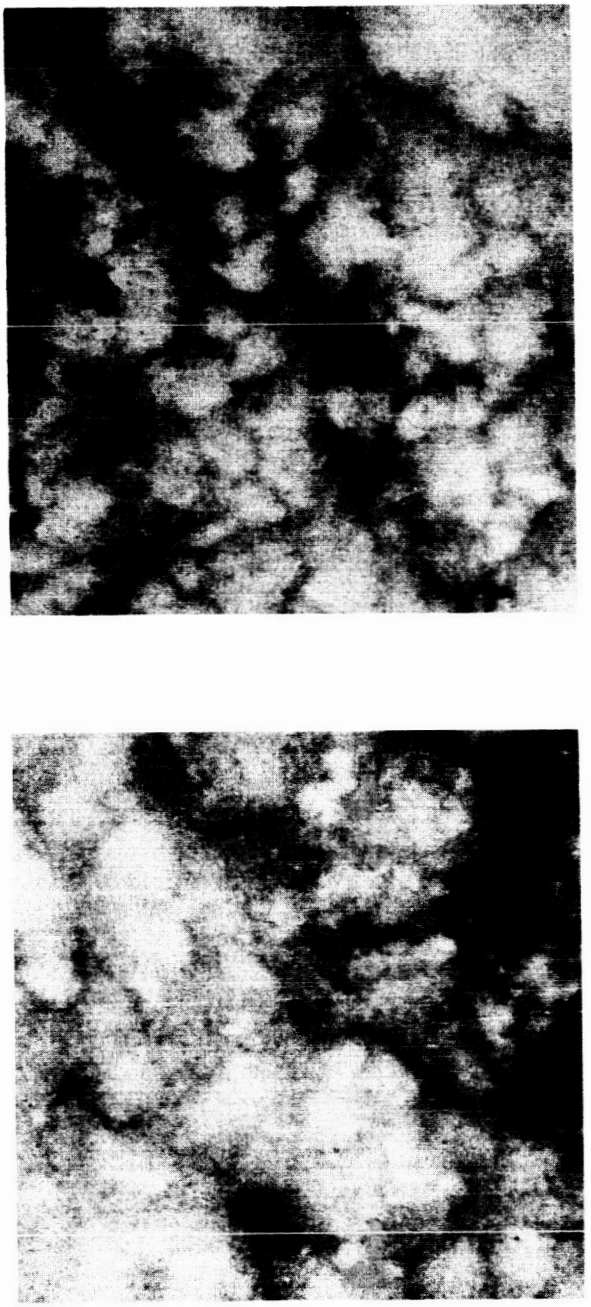

CZ010

Figure 2. Cumulus, Solid Cell

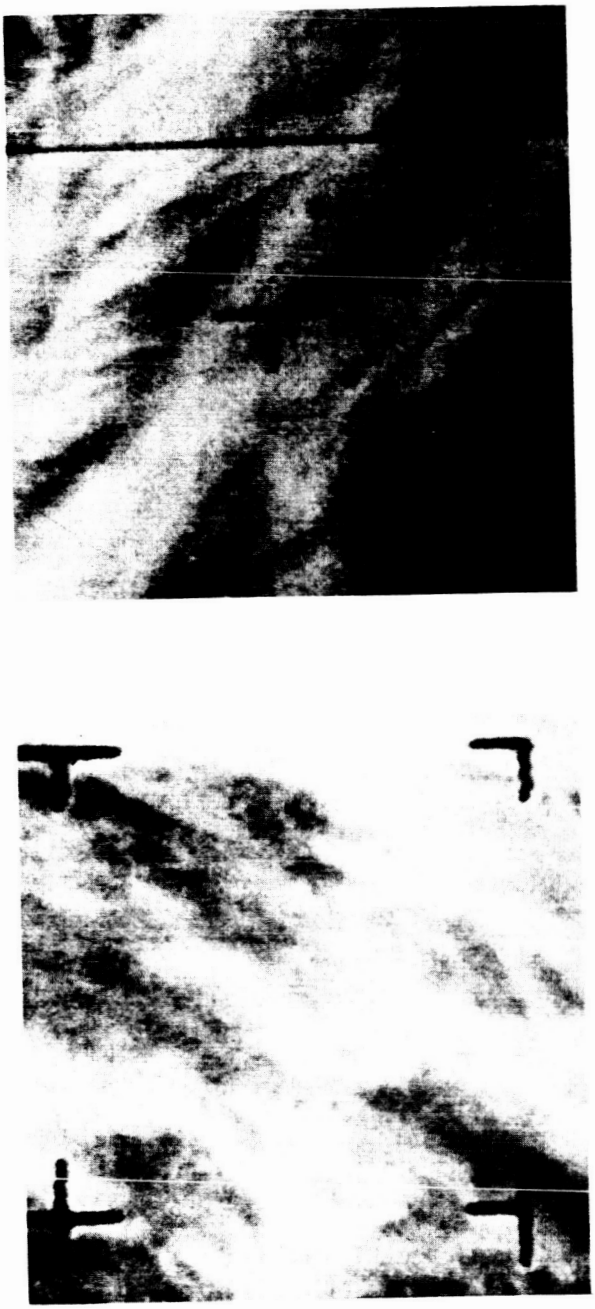

C2011

Figure 3. Noncumulus

of four adjacent points for three rows and dividing by 12 to obtain an average gray scale to represent the area originally covered by the 12 points.

An editing program was also employed to provide several translations and a 180^{o} rotation of the stored patterns to expand the pattern files. The dimensions of the video patterns actually recorded were about 35 percent greater than the required aperture size. In editing the training set six sample patterns were obtained from each recorded frame. The first aperture was centered in the frame, the second translation shifted the aperture upward by 11 resolution points in the video frame, and the third translation shifted the aperture downward by 11 resolution points. The frame was then rotated 180^{o} and the three translations were repeated. For the generalization set only the central position and 11 point upward shift were used in each rotation. The editing process produced a set of 1000 training and 200 independent test patterns for each of the three basic pattern sets.

The only assumption introduced in the course of processing the NIMBUS patterns was that the amount of light entering the vidicon aboard the satellite could be controlled electronically to maintain a constant average brightness for the received pictures. This assumption permitted adjustment of the brightness levels of the digitized photographs to compensate for variation in video gain inherent in the slow scan television system used for conversion of the pattern photographs. There appeared to be no preferred rotational orientation of the NIMBUS photographs as was the case for the lunar features and their characteristic shadow patterns. No attempt was made to preserve a particular angular relationship with the sun. No size normalization of the patterns was performed.

The prints supplied were enlarged from 35 mm negatives on 8 in. x 10 in. contrast grade 3 paper. The correct gray scales were maintained during the printing process through the use of a densitometer positioned under a particular square in the middle of the gray scale wedge associated with each photograph. On most of the prints from six to eight gray levels were discernable on this gray scale wedge.

To obtain an estimate of resolution and aperture size required for recognition of the cloud patterns, typical examples were selected from the

three pattern groups and placed before the slow scan television camera. The monitor display was photographed as the distance between the TV camera and the pattern was increased in several steps. The photographs were examined to determine the minimum size aperture with which the various patterns could be recognized. These apertures corresponded to a 0.9-inch square on the original 6 by 6 inch photographs of noncumulus patterns and a 1.4 inch square on the original polygonal cell and solic cell cumulus photographs. It was also felt that the 50 resolvable elements across the aperture did not give sufficient detail to recognize individual cells in the cumulus patterns. The digital pattern processing program was modified to achieve a resolution of 75 elements across the aperture (field of view of the recognition system). The small size of the aperture made it possible to choose several examples of the cloud features from each photograph. Thus, of the 311 prints originally provided, only the 147 prints judged by Astropower to contain the best examples of the selected features were used for conversion to video patterns.

With the smaller aperture used for the noncumulus photographs it was possible to avoid areas of the NIMBUS pictures containing fiducial marks; however, the larger aperture required for the cumulus patterns included at least one fiducial mark at any position on the photograph. Also many of the photographs contained long black lines running across the areas of interest. Since these extraneous marks appeared as strong features and could confuse the classification problem, it was considered desirable to eliminate them. A water color retouching kit was used to cover the marks and an attempt was made to match the gray scale and pattern shape of the area surrounding each mark. The upper photograph in Figure 1 contains three unretouched fiducial marks and one retouched mark. The lower photograph contains two retouched fiducials and a retouched black line. Figure 3 contains examples of unretouched fiducial marks and black lines.

3.0 EXPERIMENTAL PROGRAM

3.1 Introduction

The three pattern classes as previously described are: cumulus solid cells, cumulus polygonal cells, and noncumulus cloud cover. The recognition tasks were to: (1) separate the cumulus from noncumulus clouds and (2) separate the cumulus solid cells from the cumulus polygonal cells. This seems to be the most natural processing, although an examination of the patterns indicates that first splitting off the polygonal cells and then separating the solid cells from the noncumulus cover would provide easier recognition tasks.

Unlike the lunar patterns, the NIMBUS features cover the entire sampling aperture. Thus the lunar features can be centered in the field of view, but the NIMBUS patterns cannot. Unless the classes can be separated by the average gray level of the patterns, the linear property filters generated by the simple discriminant analysis (SDA), described in the previous report, will give poor performance on uncenterable patterns. The linear units provided poorer performance than the quadratic units (DAID) on the lunar features which could be centered. For these reasons, only the quadratic units were used in the NIMBUS experiments.

For each of the two NIMBUS tasks, a set of 400 quadratic property detectors, each unit having 7 input connections, was derived. As described in TPR-2, the specification of these units is accomplished by a program which designs an entire recognition network. Due to some computational shortcuts in this program, instabilities arose in the design of the network for separating the solid cells from the polygonal cells. The set of property filters for this task is comprised of the initial segments of three networks, these segments consisting of 70, 160 and 170 units. The set of filters for the cumulus-noncumulus task comes from a single network.

Decision mechanisms were designed for the sets of property filters using the six adaptive techniques described in the last report (Forced Learning, Bayes Weights, Error Correction, Iterative Design, Madaline, and Mean Square Error). The last four are recursive routines and were modified to compute the classification and generalization performance levels after each cycle. The results of the NIMBUS experiments are presented in a somewhat

different format than for the lunar experiments, reflecting the additional information provided by these changes.

The design runs for the decision mechanisms were longer than for the lunar experiments. The Iterative Design Procedure was run on an SDS 930 for 13 hours for the first task and 8 hours for the second. The MADALINE design was run for 9 and 16 hours, respectively. The MADALINE system used 3 ADALINES instead of the 7 used on the lunar tasks. This, combined with the longer run brought the MADALINE performance levels up to the best in the group. The Error Correction procedure was run for 10 and 19 hours and the Mean Square Error for 10 hours on each task.

3.2 NIMBUS Experiments

3.2.1 Cumulus vs. Noncumulus

The first task considered for the NIMBUS data is the separation of cumulus from noncumulus cloud cover. As in the lunar experiments, 1000 samples of each class are used as training patterns, and an independent sample of 200 patterns of each class is used to test generalization. These 1200 are derived from a smaller set of basic patterns by translation and rotation. The patterns are presented as a 75 by 75 array, in contrast to the 50 by 50 array used in the lunar experiments.

Four hundred quadratic property filters were derived for this task. This number was selected primarily on the basis of computer time available. The iterative design algorithm is able to separate the training patterns completely, demonstrating that the property profiles of the patterns are linearly separable.

The performances achieved by the six adaptive techniques are shown in Figure 4. For the four recursive techniques, two blocks of data are shown. The first block shows the cycle in the recursive process at which the best performance on the training patterns is achieved, and the classification and generalization performance at that point. The second block indicates the cycle and performance levels for best generalization performance. The total number of cycles examined is also indicated.

Technique	Classification %	Generalization %
Forced Learning	78.00	81.25
Bayes Weights	77.90	82.50

	Total Cycles	For Best Classification			For Best Generalization		
		Classif. %	Gen. %	Cycles	Classif. %	Gen. %	Cycles
Error Correction	365	95.15	81.75	81	92.20	85.75	6
Iterative Design	78	100.00	84.25	78	93.45	86.25	2
Mean Square Error	48	83.70	78.50	1, 12	83.70	78.50	1, 12
Madaline	63	100.00	85.50	63	99.80	86.00	59

c1958

Figure 4. Cumulus vs. Noncumulus – 400 DAID Units

Both the iterative design and MADALINE achieved perfect separation of the training patterns. Iterative design shows the patterns to be linearly separable. Despite a very long run (19 hours), error correction did not achieve complete separation, although it is eventually guaranteed to do so.

The best generalization performances are achieved by iterative design, MADALINE, and error correction. The other recursive technique, mean square error fails to achieve even the levels of the non-recursive forced learning and Bayes weights. Iterative Design and error correction achieve their best generalization performance very early in the design. This has been observed consistently, and may be characteristic of these two techniques.

Of the three high performance techniques, MADALINE shows the least sacrifice in generalization performance when classification performance is used as the criterion for terminating the design. This, of course, is a desirable feature. This observation may be related to the early peaking of generalization for iterative design and error correction. Iterative design shows a moderate drop-off, while the performance for error correction falls below the level achieved by Bayes weights.

Figures 5 through 8 show the performance of the four recursive techniques on a cycle by cycle basis (up to 100 cycles). The solid lines represent classification performance, the broken lines show generalization performance. Best performance points are indicated by small triangles under the curves. Although the error correction and MADALINE curves show more irregularity than the iterative design and mean square error curves, the degree of irregularity is not typical. The error correction and MADALINE curves of the next section show greater irregularity, and are more typical. The greater the irregularity, the more difficult it is to choose the best stopping point for the design process. Generally, the peaks and valleys of the generalization curve tend to coincide with peaks and valleys of the classification curve.

3.2.2 Solid Cells vs. Polygonal Cells

The performance figures obtained on the task of separating the solid cell patterns from the polygonal cell patterns are very similar to those cumulus-noncumulus tasks. The results appear in Figure 9.

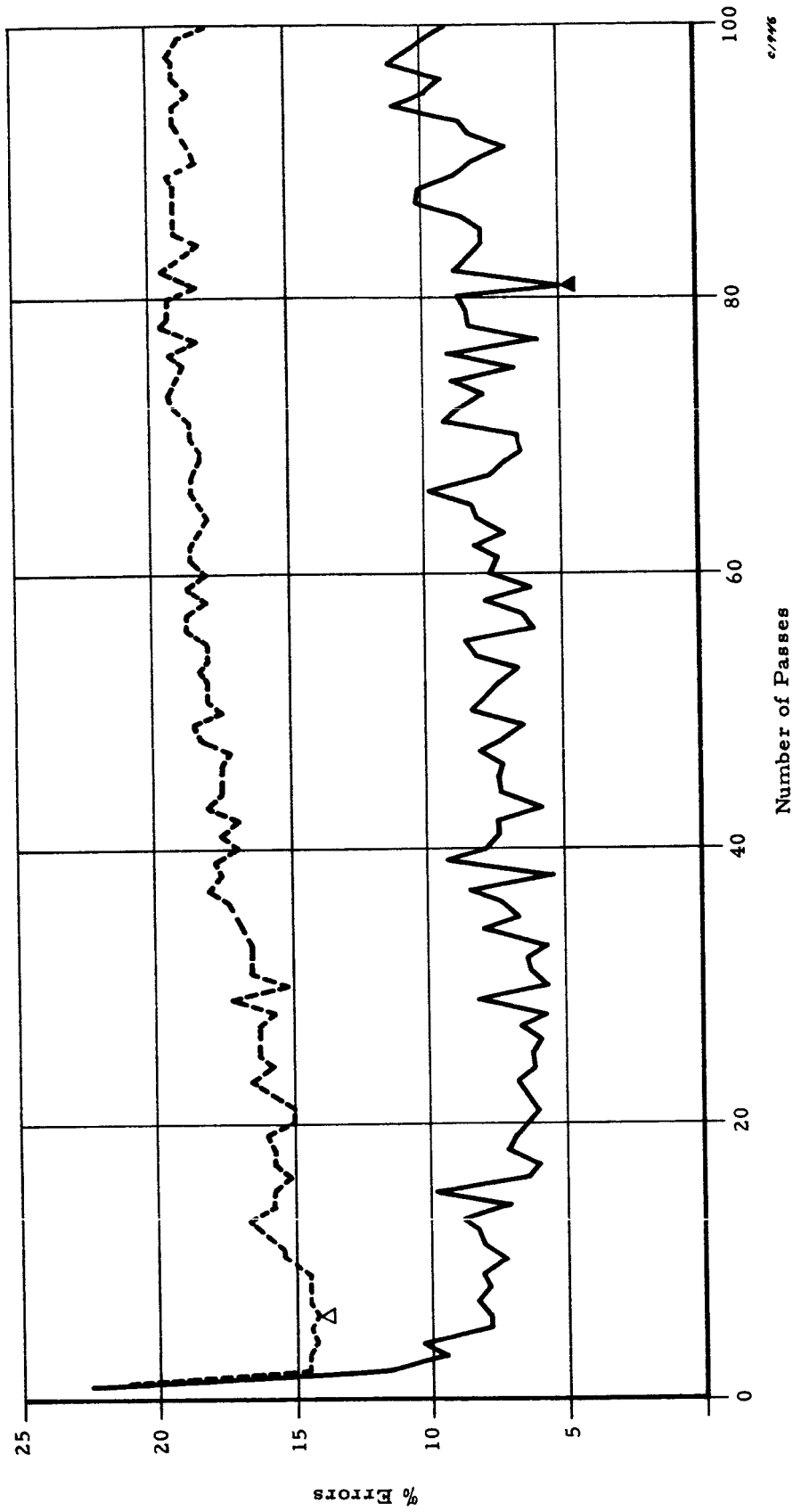

Figure 5. Error Correction — Cumulus vs. Noncumulus

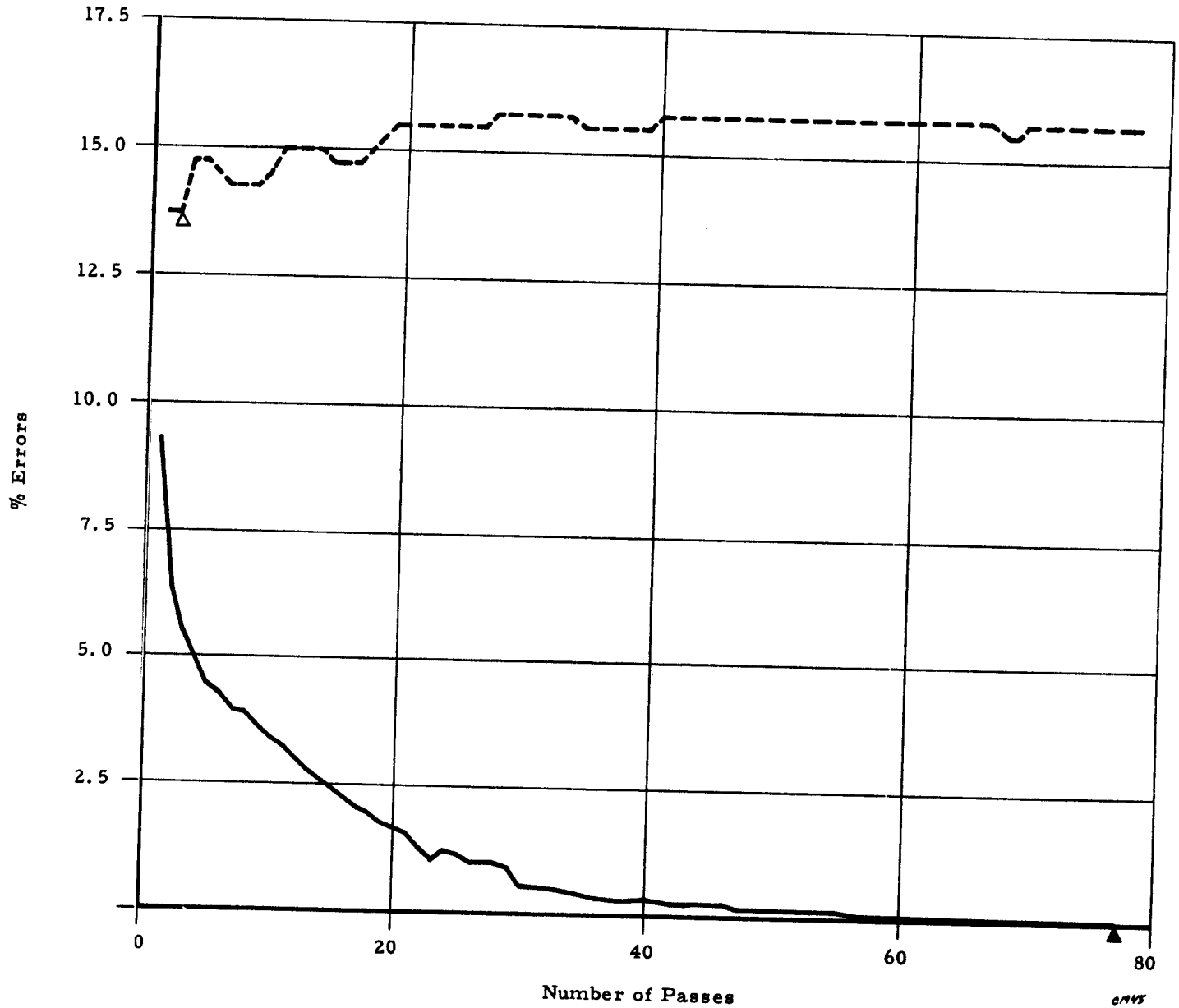

Figure 6. Iterative Design – Cumulus vs. Noncumulus

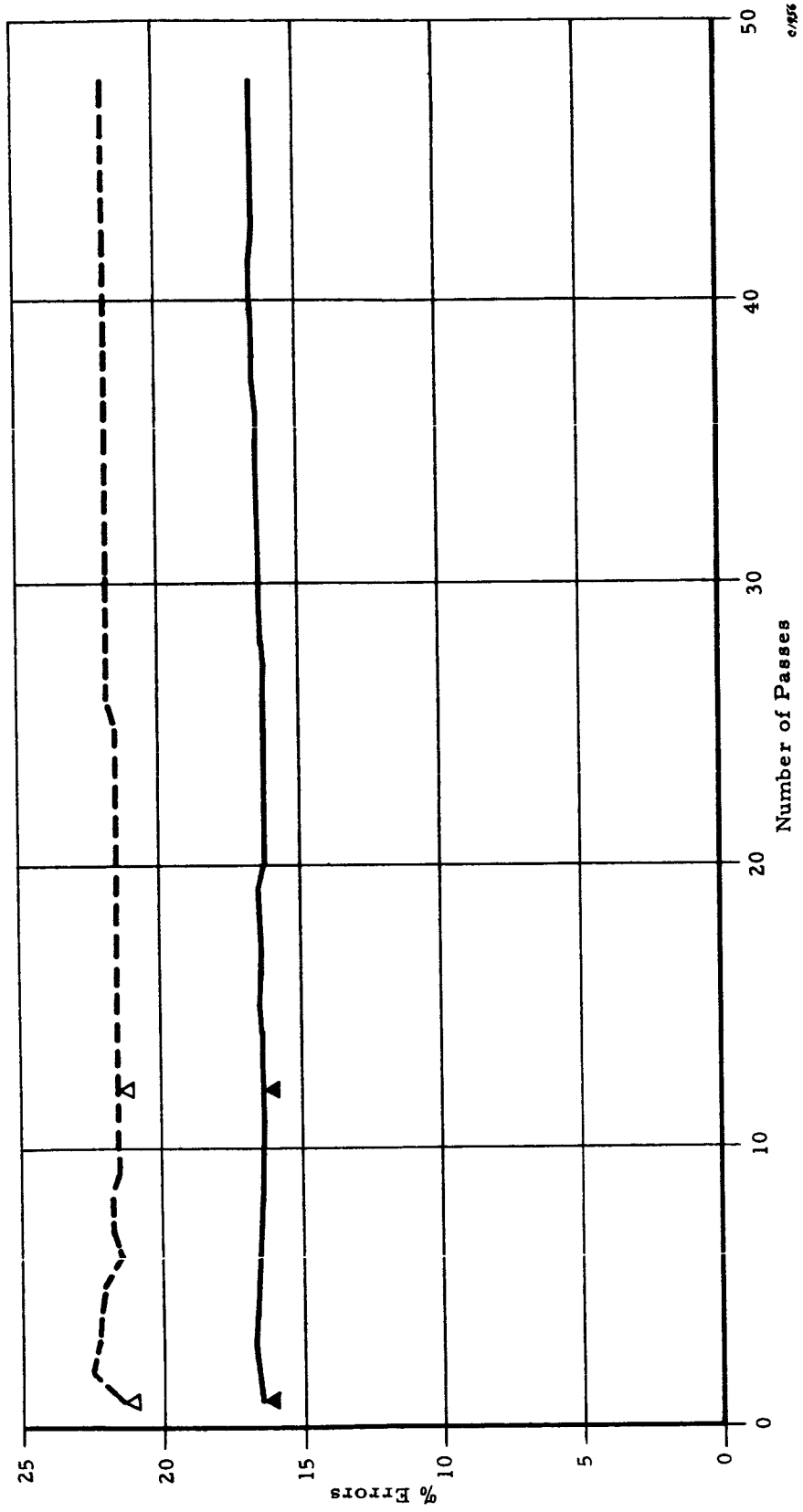

Figure 7. Mean Square Error — Cumulus vs. Noncumulus

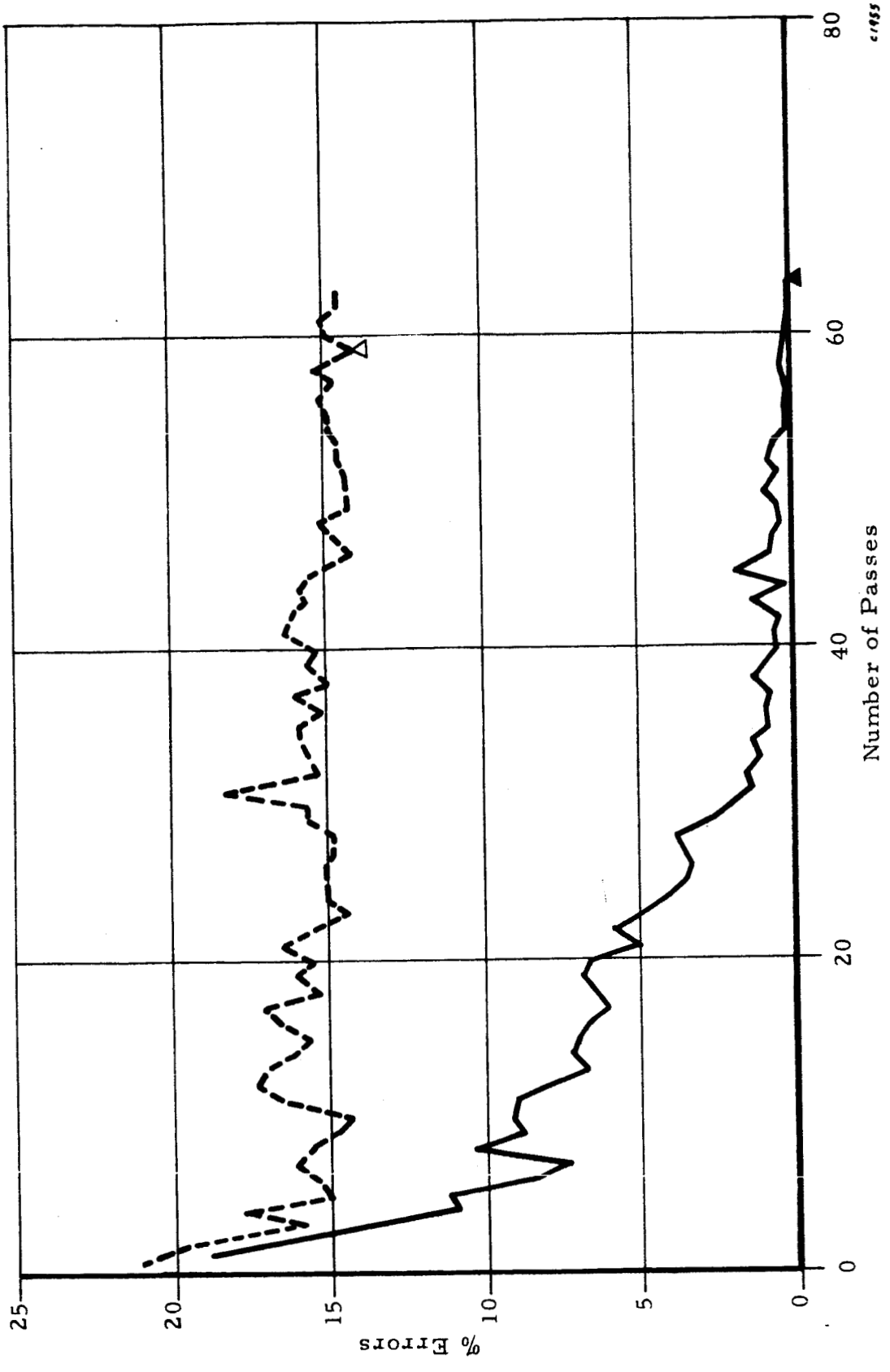

Figure 8. Madaline – Cumulus vs. Noncumulus

Technique	Classification %	Generalization %
Forced Learning	86.10	81.00
Bayes Weights	86.10	82.00

	Total Cycles	For Best Classification			For Best Generalization		
		Classif. %	Gen. %	Cycles	Classif. %	Gen. %	Cycles
Error Correction	192	92.40	80.50	34	89.30	83.00	1
Iterative Design	47	98.50	82.75	47	90.50	85.50	1
Mean Square Error	49	86.95	80.75	25-49	86.95	80.75	25-49
Madaline	112	99.85	85.00	76	97.40	85.50	72

Figure 9. Solid Cells vs. Polygonal Cells – 400 DAID Units

Complete separation of the training patterns was not obtained but the MADALINE and iterative design techniques both achieved less than 2 percent error rate. These two techniques also provided the best generalization performance. Error correction and iterative design again exhibit their best generalization early in the design. As before the MADALINE shows the least sacrifice in generalization when classification performance level is used to terminate the design process. Iterative design performance falls almost to the level of Bayes weights, and error correction falls noticeably below that level.

Figures 10 through 13 show the cycle by cycle performance for the recursive techniques. The greater irregularity of the MADALINE and error correction curves appears to be more typical of the results in this study than those of the preceding section.

The set of 400 property detectors was obtained from three network designs. The first subset consisted of 70 units. Decision functions for just these 70 units were derived using each of the six adaptive techniques. The performance figures are given in Figure 14. Generalization performances are better than for the 400 unit system in all but one case (MADALINE, when the design is stopped to give best classification performance). The performance figures are remarkably similar for five of the six techniques, the exception being mean square error. With 70 property detectors, the classification and generalization performance levels are virtually identical. This suggests the possiblity that the first 70 units extract the important statistical properties of the training patterns, and that the additional units utilize quirks in the training patterns to aid classification of these patterns, but are irrelevant in generalization.

The generalization performance sacrifice caused by stopping for best classification performance produces an ordering of the three good recursive techniques which is opposite to the earlier cases. Thus sacrifice is least for error correction, greatest for MADALINE. As in the earlier cases, error correction and iterative design achieve their best generalization performance early in the design.

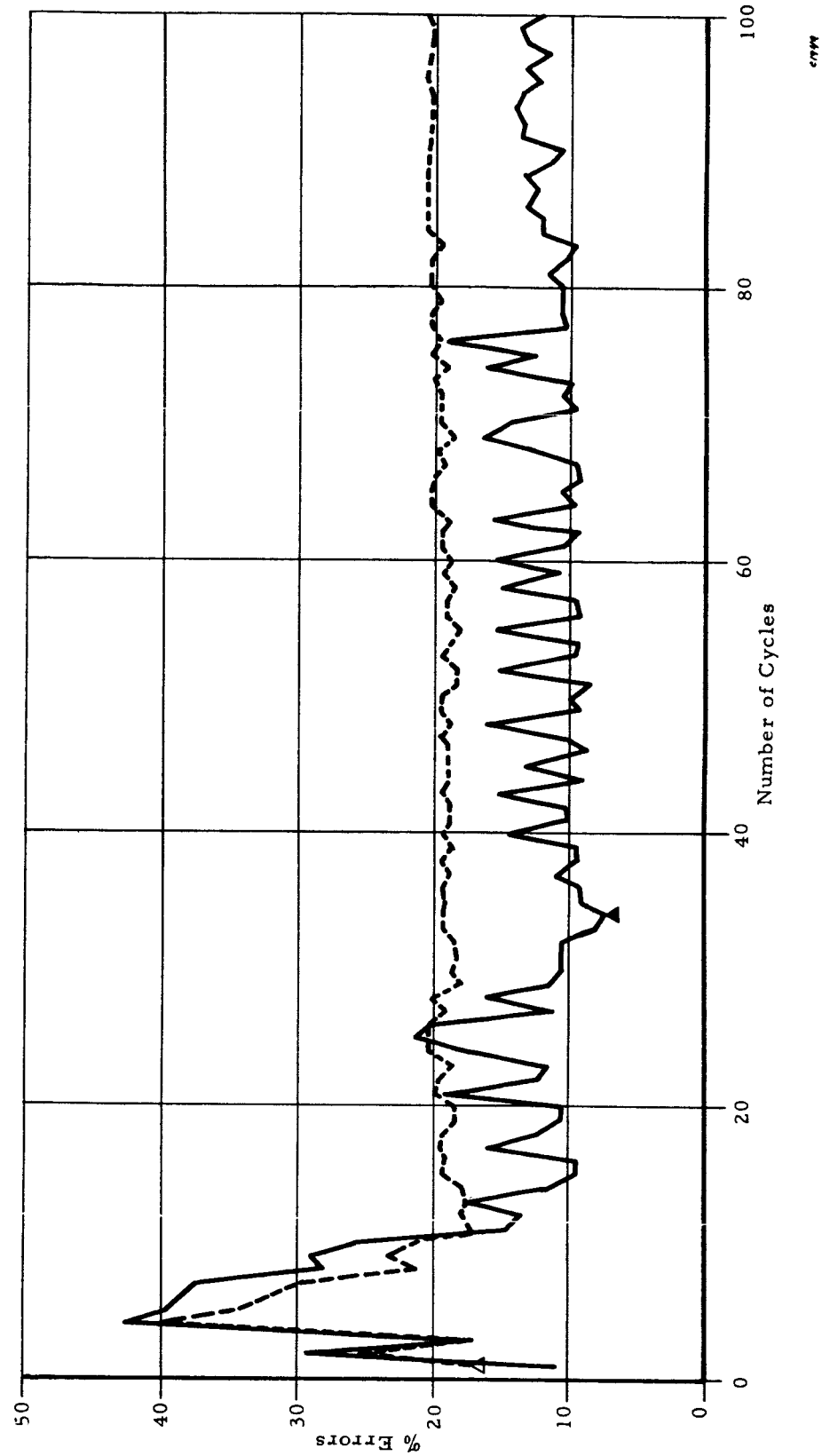

Figure 10. Error Correction— Solid Cells vs. Polygonal Cells

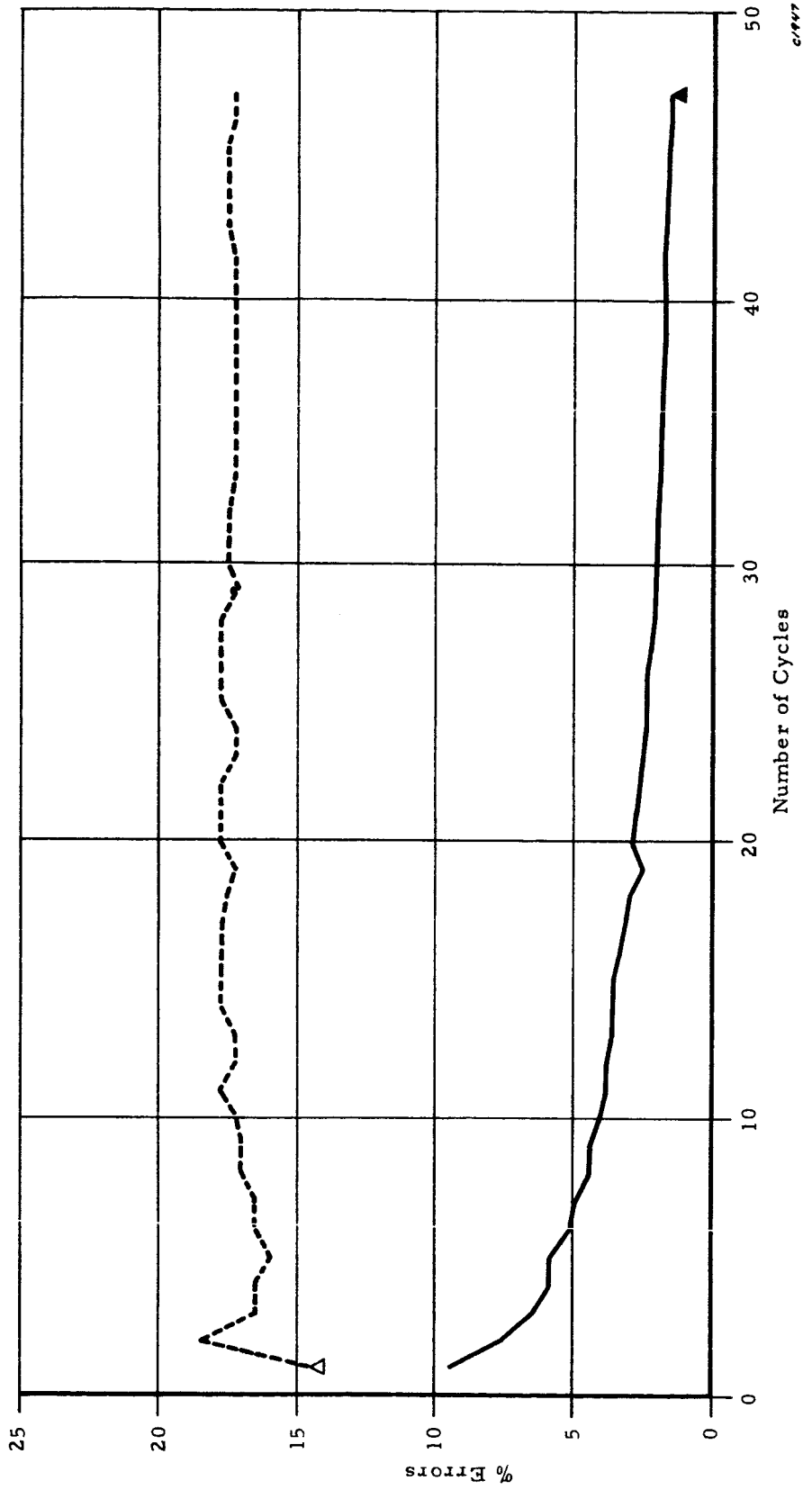

Figure 11. Iterative Design — Solid Cells vs. Polygonal Cells

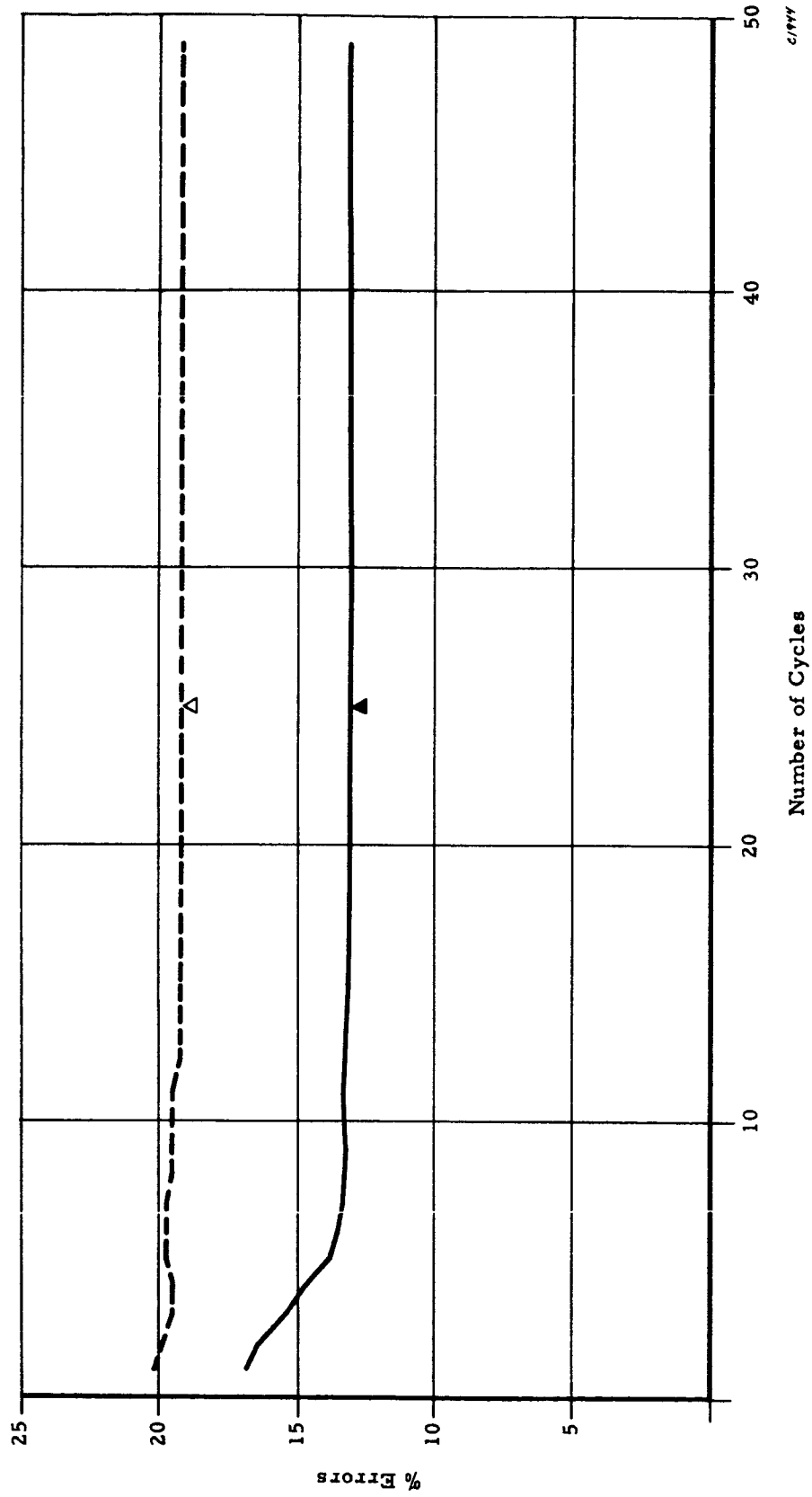

Figure 12. Mean Square Error — Solid Cells vs. Polygonal Cells

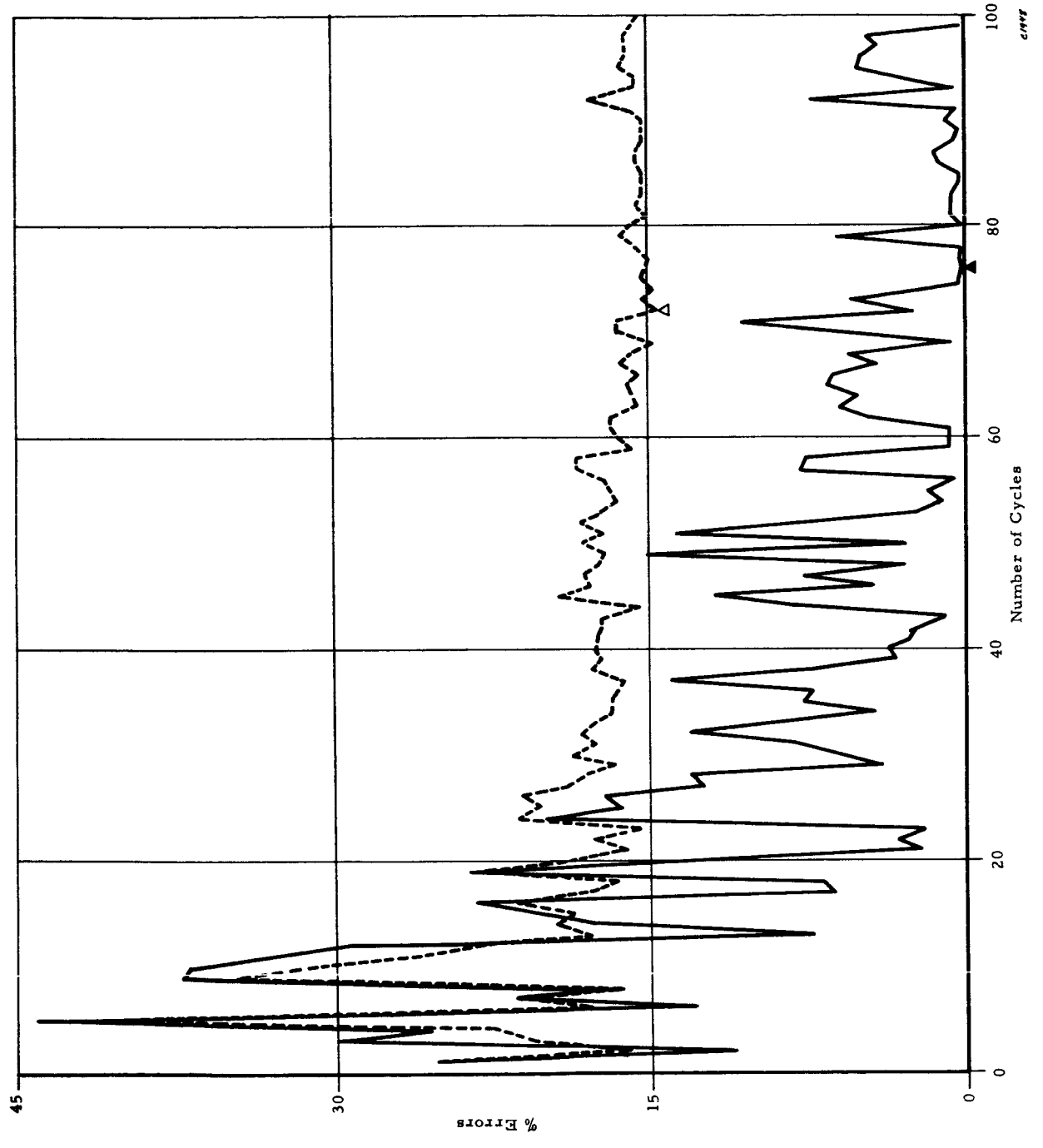

Figure 13. Madaline – Solid Cells vs. Polygonal Cells

Technique	Classification %	Generalization %
Forced Learning	85.50	86.25
Bayes Weights	85.65	85.75

	Total Cycles	For Best Classification			For Best Generalization		
		Classif. %	Gen. %	Cycles	Classif. %	Gen. %	Cycles
Error Correction	93	86.65	85.00	52	86.05	86.25	6
Iterative Design	45	87.05	85.00	41	86.25	87.00	5
Mean Square Error	8	83.65	84.25	2-8	83.65	84.25	2-8
Madaline	114	86.95	84.25	67	85.70	87.25	46

C/957

Figure 14. Solid Cells vs. Polygonal Cells – 70 DAID Units

Additional experiments were performed using 50 units, but poorer generalization resulted. Experiments with 70 units for the cumulus-noncumulus discrimination also yielded performances poorer than those already available.

3.3 Multiple "Looks"

For three of the four pattern categories in the NIMBUS tasks, the generalization sample of 200 patterns per class were derived from 50 basic patterns for each class. The basic patterns were sampled at two translations for each of two rotations. Thus, there are four "looks" at each of the 50 basic patterns for these classes. For the remaining category, Cumulus, 100 basic patterns were sampled at two rotations, providing two "looks" at each pattern.

The possibility of improving generalization performance by combining the decisions of the several looks* was investigated for the forced learning, Bayes weights, and iterative design. The method consisted of simply summing the values of linear decision functions for all of the looks. The results are given in Tables III and IV.

TABLE III

GENERALIZATION PERFORMANCE – CUMULUS VS. NONCUMULUS

	Forced Learning	Bayes Weights	Iterative Design
100 Cumulus (2 look)	86.0 (86.0)	84.0 (87.0)	87.0 (85.0)
50 Noncumulus (4 look)	82.0 (76.5)	82.0 (78.0)	92.0 (87.5)
150 Overall	84.7 (81.25)	83.3 (82.5)	88.7 (86.25)

The original (single look) performance is shown in parentheses.

*This approach was suggested by J. H. Munson of the Stanford Research Institute, who uses nine looks at each pattern, computes a decision for each look, and derives a majority decision. His method is thus similar to a MADALINE in which the ADALINES compute similar functions.

TABLE IV

GENERALIZATION PERFORMANCE – SOLID CELL VS. POLYGONAL CELL

	Forced Learning	Bayes Weights	Iterative Design
50 Solid Cells (4 look)	76.0 (73.5)	76.0 (73.5)	80.0 (77.0)
50 Polygonal Cells (4 look)	96.0 (88.5)	96.0 (90.5)	98.0 (94.0)
100 Overall	86.0 (81.0)	86.0 (82.0)	89.0 (85.5)

If the decisions for the different "looks" were completely dependent, that is, the correctness of the decisions depends only on pattern difficulty and not on its location or orientation, one would expect no change in performance. If the looks were completely independent, one might compute the expected performance as follows. Over the sample patterns in a category, the linear decision function may be considered to be approximately normally distributed. To achieve 80% performance the magnitude of the mean to standard deviation ratio should be 0.84. Considering the sum of two such independent variables, the mean is doubled, but the standard deviation is multiplied by $\sqrt{2}$. Thus the ratio is multiplied by $\sqrt{2}$. For four independent "looks," the mean is quadrupled and the standard deviation doubles. Thus the ratio doubles. The expected performance for two looks in this case is 88.3% and for four looks 95.3%. Table V gives some typical values.

TABLE V

EXPECTED PERFORMANCE FOR INDEPENDENT LOOKS (%)

Single Look	Two Look	Four Look
75	83.5	91.6
80	88.3	95.3
85	92.9	98.1
90	96.5	99.5
95	99.0	99.95

The performance levels actually achieved are greater than the single look levels, but are much closer to these values than those to be expected if the looks were independent. This indicates that the original decisions are somewhat, but not greatly, dependent on position and orientation. The use of a larger training sample is suggested.

The multiple look method may be implemented by sequential processing, or by the inclusion of four times as many property filters, or by a combination of these methods.

3.4 Evaluation

This section summarizes the results of the various recognition experiments performed and presents an evaluation of these results.

1. The generalization performance levels achieved are sufficiently high to encourage further development of a spaceborne system. The 90 percent correct recognition achieved is very similar to the performance obtained in a NASA in-house effort using known properties and statistically derived decision functions.

2. MADALINE was one of the two techniques offering the highest performance levels. It has the advantage that it usually provided a negligible loss in generalization performance when best performance on the training patterns is used as the criterion for terminating the design process. It has the disadvantages of requiring three times as many adjustable weights as the other techniques and longer design times due to the inefficient algorithm and the late occurrence of the optimal performance points.

3. Iterative design was the other high performance technique. It has the advantage that best generalization usually occurs very early in the design process, offering the possibility of very short design times. Further design improves performance on the training patterns in a very smooth fashion, while similarly decreasing the generalization performance. The smoothness of the curves makes the selection of the optimum point for stopping less critical. Generalization performance loss when classification performance is used as the stopping criterion is moderate.

4. Error correction offered performances as high as MADALINE and iterative design on about half the tasks, and intermediate levels on the other tasks. It shares with iterative design the advantage of early peaking of the generalization performance. Generalization loss was usually the largest of these techniques with classification as the stopping criterion. As with MADALINE, performance curves are irregular, making stopping point selection more critical; and the algorithm is inefficient, improving classification performance very slowly.

5. The remaining three techniques — forced learning, Bayes weights and mean square error — usually offer substantially lower performance levels. The first two of these techniques offer the advantage of being non-recursive.

6. The multiple look analysis indicates that the discrimination capability of the property filters is somewhat dependent upon translation and rotation of the patterns. This may be remedied by including more translations and rotations in the set of training patterns so that the property filters derived are less sensitive to these pattern changes, and/or replicating the property filters derived in other translations and rotations to implement the multiple look technique.

7. There is some evidence that the sets of property filters are too large. On one task, the first 70 property filters (approximately) appear to have extracted all of the significant statistical information that was obtained from the training patterns which aid classification but not generalization.

4.0 FEASIBILITY STUDY OF AN ON BOARD RECOGNITION SYSTEM

4.1 Introduction

The advanced NIMBUS Automatic Picture Taking System (APT) was conceived to permit meteorologists to obtain satellite cloud pictures in their immediate areas of interest. Each picture is slow scanned by a vidicon which completes the scanning operation in approximately 200 seconds. During picture scanning, a continuous broadcast of the scanned pictorial information is made from the satellite. Near-polar orbits of the NIMBUS are calculated to provide complete (daylight) coverage of the earth – the satellite passes over almost every location on earth at local noon and midnight.

In the system being studied, processing of the cloud pictures is to be done onboard the satellite and only the very limited amount of information necessary to describe the cloud cover is transmitted back to earth.

Although the APT system is fundamentally different in concept, it provides useful estimates for system parameters such as input light conditions and the time available for processing the picture.

Picture processing is to be accomplished by a recognition system which classifies a small subregion of the input picture as a specific type of cloud formation. Consistent with the experimental program discussed in previous sections, only four classifications will be considered for this discussion:

Class 1. Image subregion contains noncumuloform cloud cover.
Class 2. Image subregion contains cumuloform solid cells.
Class 3. Image subregion contains cumuloform polygonal cells.
Class 4. Image subregion contains no cloud cover.

It is convenient to partition the recognition system into three parts as shown in Figure 15. The preprocessor performs the following functions:

1. Stores the input image.
2. Scans a subregion of the stored image.
3. Transforms the output of the scanner into a form acceptable to the recognition device.

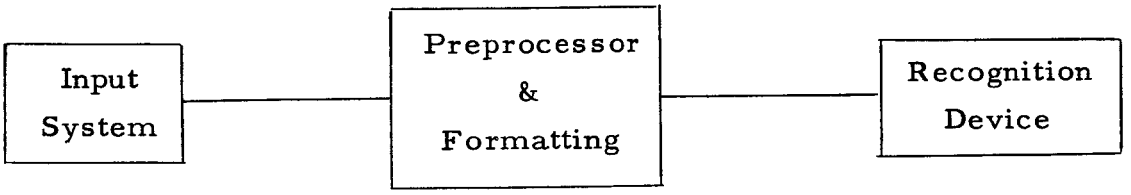

Figure 15. Recognition System

The recognition device operates on the output of the preprocessor and determines the classification of the subregion.

In studying possible implementations of the recognition system two variations of a parallel/analog system are initially investigated. Each of these approaches involves a hardware technique for providing the output of the preprocessor in the parallel format required by an analog realization of the recognition device. Wherever possible, off-the-shelf components are considered.

In the parallel/analog system the input image (provided by an input lens and variable aperture) is stored on an image storage tube. Scanning of a subregion of the stored image is accomplished by means of a dissector tube. The requirement that the inputs to an analog recognition device be available in parallel can be met by

1. Converting the output signal from the dissector tube back into an image through the use of a display storage tube which is then sampled by a photosensitive array.
2. Sequentially sampling the output of the dissector tube and storing the samples in a capacitor bank. The elements of the bank can be simultaneously interrogated to provide the necessary parallel format.

For the hardware realization of an analog recognition device, 400 quadratic logic units are used in the first layer and two linear logic units in the second layer. The linear units do not present a difficult design problem. On the other hand, lightweight quadratic units with consistent performance are not available. A promising design for a quadratic logic unit has been investigated and its performance (for positive inputs only) is discussed.

The image processing technique under consideration assumes that each input image yields 121 square subregions arranged so that there is a 50% overlap in the vertical and horizontal directions. After each subregion is processed onboard by the recognition system, the classification of each of the 121 subregions is transmitted back to earth.

For each of the two systems considered the size, weight and power required is estimated. In the cases where a given system component is not an off the shelf item, its performance and utility is based on present state of the art technology.

4.2 Image Storage and Subregion Scanning

A Tegea (f:1.8, 26 mm) lens similar to that used in the NIMBUS APT system is suitable as the input lens for the systems being studied. The image format provided by the lens is a square with a 1.5 inch diagonal to yield a 108° field of view. The output of the lens is electronically shuttered to yield an exposure time of one msec on the image storage tube.

The image formed by the lens is retained by the image storage tube and subregion scanning is performed by the image dissector tube. The input system configuration is shown in Figure 16.

4.2.1 Image Storage

The image storage tube operates essentially as an electronic camera. A diagram of this tube with typical auxiliary equipment is shown in Figure 17. The image storage tube operates in three modes: (1) erase, (2) write, and (3) read. The backing electrode is similar to a screen coated with dielectric material. During all phases the collector electrode and the viewing phosphor are maintained at a fixed positive bias with respect to the photocathode. In the erase mode the backing electrode potential is increased slightly above the normal reading potential, the light source illuminates the photocathode and the photocathode is set at zero potential. The step increase in potential on the backing electrode causes the dielectric material to charge positively due to normal capacitor action. During this interval electrons are bombarding the backing electrode since the light source is at this time providing photons to the photocathode. This electron bombardment causes the potential of the positively charged dielectric mesh to be reduced. In time, the dielectric side of the backing electrode reaches a uniform equilibrium potential of zero volts corresponding to the potential at the photocathode. This essentially constitutes erasure.

In the write phase the external light source is turned off, the photocathode to collector accelerating potential is increased, and the backing electrode reduced to zero. The negative transient at the backing electrode causes a large negative voltage to appear on the adjoining dielectric material. The increase in photocathode to collector electrode potential causes high velocity electrons to be emitted by the photocathode and to bombard the

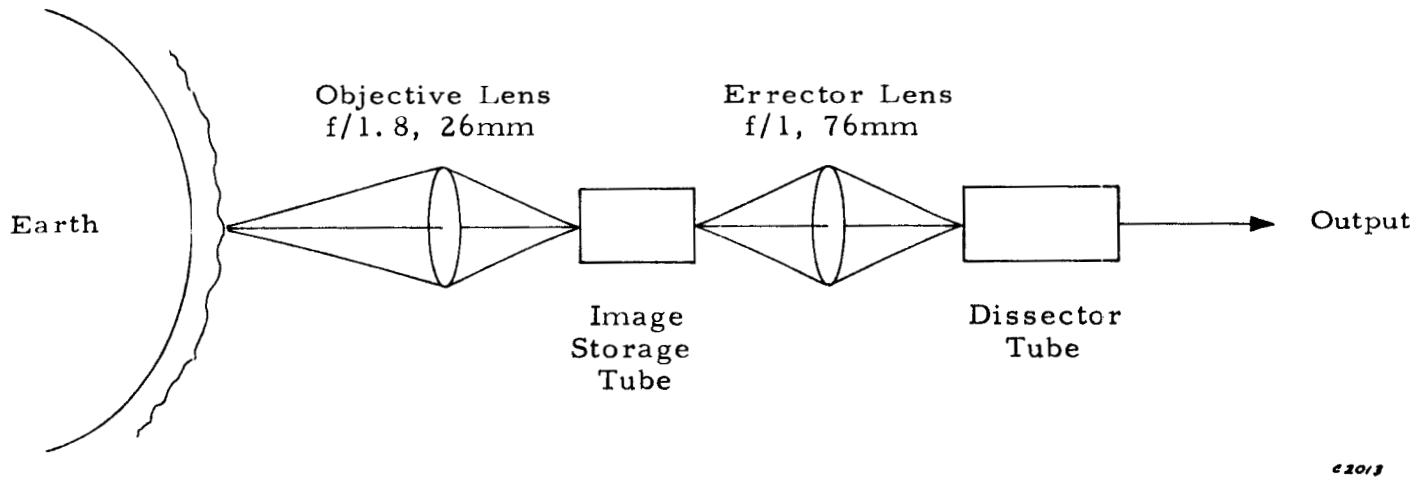

Figure 16. Input System

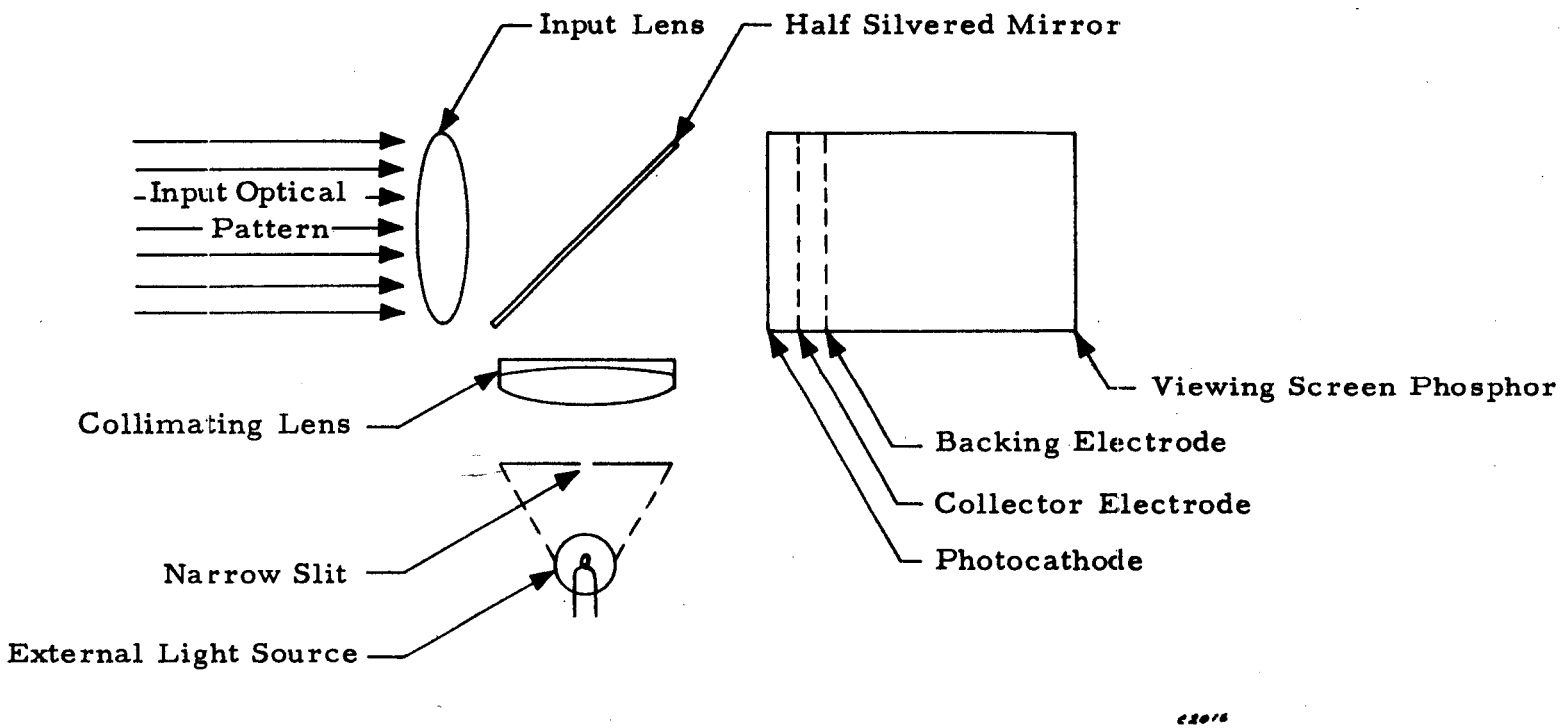

Figure 17. Image Storage Tube

dielectric material of the back electrode causing secondary emission of electrons which are absorbed by the collector electrode. A bright element in the input pattern therefore produces a positive potential on the backing electrode dielectric mesh. Reading is accomplished by again reducing the photocathode to zero potential and re-energizing the light source. Simultaneously the backing electrode potential is increased positively to allow maximum flow of the modulated electron beam passing through the dielectric mesh.

The timing diagram (Figure 18) shows the operation of a typical image storage tube such as the ITT FW 232. This tube maintains the viewing screen at 10 kilovolts and the collector electrode at plus 50 volts. The major parameters of the FW 232 image storage tube are listed as follows:

Viewing time	– 60 seconds
Erasing time	– 0.5 seconds
Allowable illumination-time (Product)	– 1 to 20 x 10^{-3} footcandles sec.
Allowable input range	– 20;1
Maximum output emittance	– 2 x 10^{-3} lumens/cm^2
Input Photocathode	– S-11
Output Phosphor	– P-20
Distinguishable levels	– 5 to 8
Resolution	– 500 TV lines/in.
Useful diameter	– 1.5 inches
Weight	– 8 lbs.
Size	– 5-5/8 in. by 5 in. O.D.

The maximum output luminous emittance of the phosphor is limited by the allowable current density of the photocathode. Typically, the maximum photocathode current density is 20 μa/$in.^2$. If greater output is required this can be achieved by scanning the photocathode with a concentrated light source during readout.

Noise in this tube arises from two sources, that is, photocathode shot noise, and variations in brightness due to nonuniform deposition of the dielectric mesh.

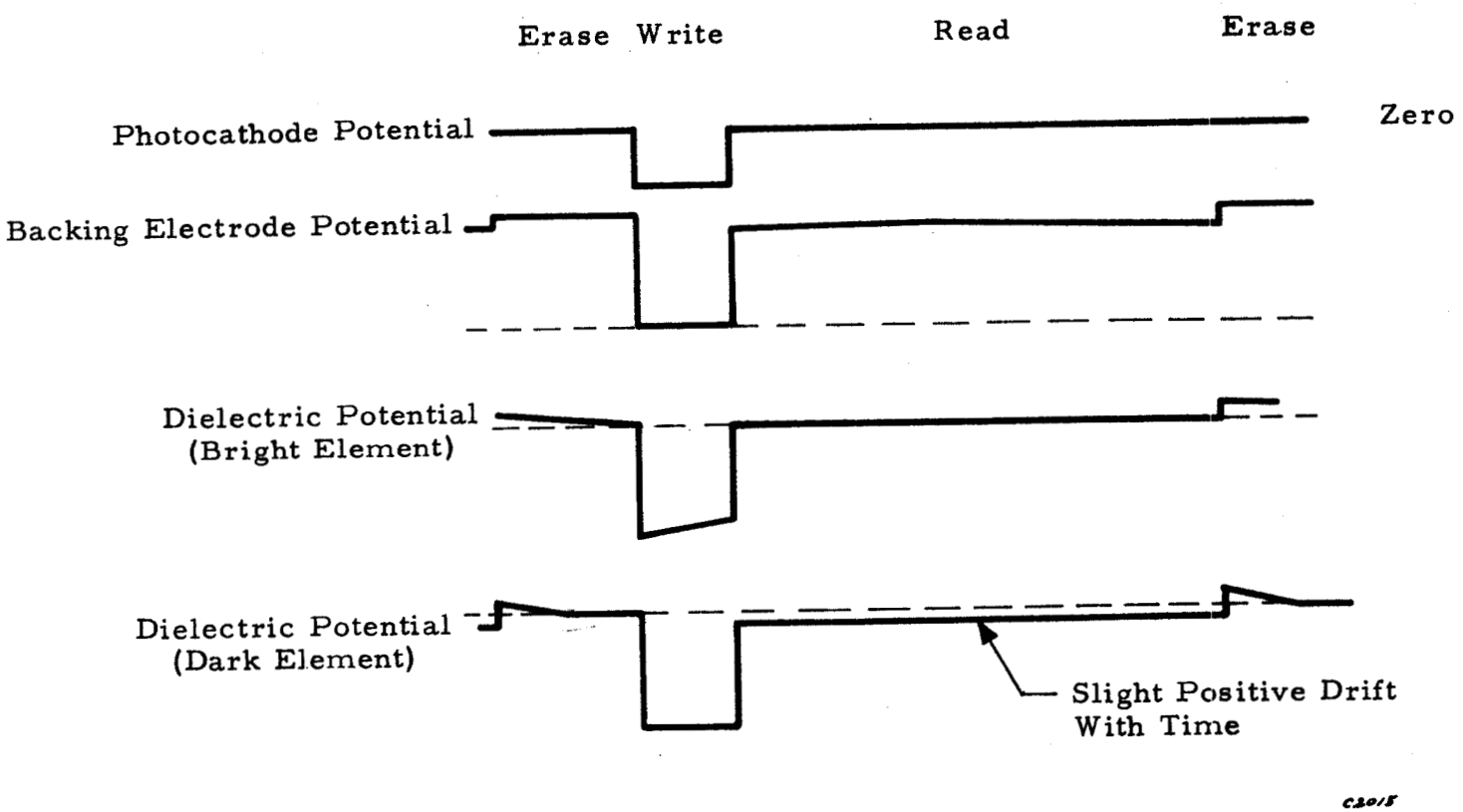

Figure 18. Timing of Image Storage Tube Operation

4.2.2 Image Dissector Tube

An image dissector tube is shown schematically in Figure 19. The photocathode of the tube releases electrons which are collimated by a magnetic focusing field in the drift tube. The direction of electron drift is dependent upon the magnetic focusing and deflection fields. An aperture (in the aperture plate) permits electrons to pass into a multiplier section. The electrons passing through the aperture are associated with a small area on the photocathode, this area being dependent upon the field in the drift tube. The electrons passing through the aperture are multiplied by a conventional dynode structure.

An example of such a tube is the ITT F4011. Some of the specifications for this tube include a maximum of 19.7 line pairs per mm resolution, a 1.1 inch diagonal image format, and a 14 stage dynode structure. The tube with associated deflection coils is contained in a cylinder eight inches long and four inches in diameter and weighs less than six pounds.

4.3 Environmental Performance

In order to assess the feasibility of the systems in which the image storage and dissector tubes are used it is necessary to determine the following:

The ability of the storage tube to operate without saturation in the exposure time of one msec (for the light conditions imposed)

The maximum current output of the dissector tube

The number of distinguishable levels in the output of the dissector tube (i.e., the ability of the dissector to reproduce gray levels)

4.3.1 Nonsaturation of the Storage Tube

The maximum allowable product of luminous flux density and time for a S-11 photocathode is given by the manufacturer's specification of the ITT FW232 to be 20×10^{-3} lumen. sec./ft^2. This specification is based on measurements using a tungsten source at 2870°K. Since the input to the system is solar energy it is necessary to modify this product in accordance with the source employed. This is accomplished by using the conversion factor of one solar lumen to four tungsten lumens giving a maximum useful

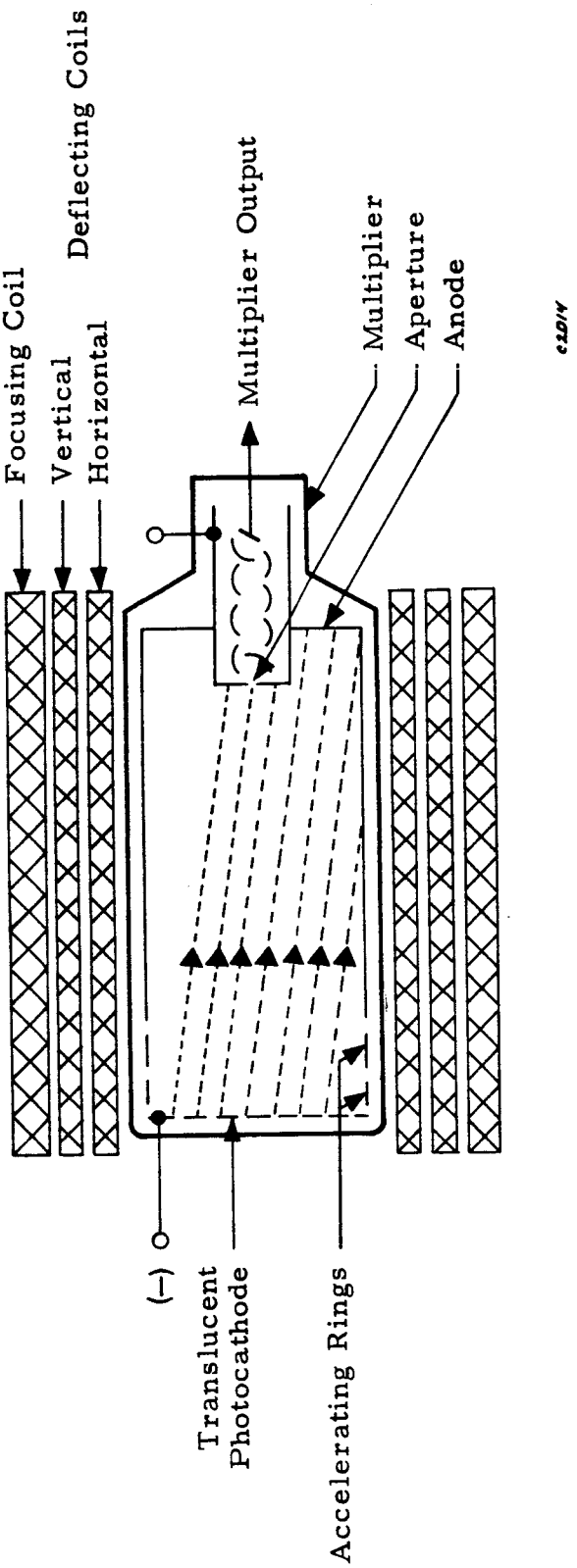

Figure 19. Image Dissector Tube

luminous flux density time product of

$$E_{max} t_e \sim 5 \times 10^{-3} \frac{\text{lumens}}{\text{ft}^2} \cdot \text{sec.}$$

where E_{max} = maximum solar luminous flux density during the exposure time t_e. The maximum output from the sun above the earth's atmosphere at mean solar distance is $12,680 \frac{\text{lumen}}{\text{ft}^2}$,[1] multiplying this number by the maximum albedo of the earth (0.9), the maximum reflected flux density obtained is $11,410 \frac{\text{lumen}}{\text{ft}^2}$.

The amount of luminous flux density gathered by the lens depends upon its f/number and transmissibility. With the lens operating at an f/number of 16 and a transmissibility of 0.7, the lens output is 7.8 lumens/ft^2. This light passes through a half silvered mirror which causes an attenuation of 0.5. The resulting maximum input to the storage tube is 3.9 lumens/ft^2. This requires that the exposure time be less than 1.28 milliseconds.

4.3.2 Output of Dissector Tube

The output current of the image dissector depends on the net output radiant flux density of the image storage tube, the spectral efficiency of the phosphor viewing screen, the lens coupling the viewing screen of the storage tube to the photocathode of the dissector tube, the sensitivity of the dissector photocathode, the dissector aperture area, and the gain of the dissector photomultiplier.

The output current may be written as:

$$I_D = a \mu \int_0^\infty W_D(\lambda) K(\lambda) d\lambda \qquad (1)$$

where

- a = aperture area (cm^2)
- μ = photomultiplier gain
- $W_D(\lambda)$ = radiant flux density as a function of wavelength (watt/cm^2) falling on the face of the dissector photocathode
- $K(\lambda)$ = sensitivity of the photocathode as a function of wavelength (amperes/watt)

The input radiant flux density (assuming a diffuse surface radiator) is:

$$W_D(\lambda) = \frac{\tau W_S(\lambda)}{4(n_f)^2 (1+m)^2} \tag{2}$$

where

τ = average transmissibility of the coupling lens over the spectrum from approximately 4700 to 7300 angstroms

$W_S(\lambda)$ = radiant flux density of the image storage tube as a function of wavelength (watts/cm^2)

n_f = ratio of focal length of the lens to the lens diameter

m = magnification required between the useful viewing screen of the storage tube and the useful photocathode of the dissector and for the system under consideration is 1.1/1.5 = 0.733.

If the spectral efficiency of the viewing phosphor is known as a function of wavelength then it is useful to express the total radiant flux density of the viewing screen phosphor as

$$W_S(\lambda) = \epsilon(\lambda) W_\tau \tag{3}$$

$\epsilon(\lambda)$ = spectral efficiency of the phosphor (watts/watt)

W_τ = total radiant flux density (watts/cm^2)

Often the luminous flux density is known rather than the radiant flux density. In this case Equation (3) may be expressed as

$$W_\tau = \frac{E_\tau}{L_e} \tag{4}$$

E_τ = total luminous flux density of the viewing phosphor (lumen/cm^2)

L_e = luminous efficiency of the viewing phosphor (lumen/watt)

Combining expressions (1), (2), (3), and (4) the resulting output current may be obtained in terms of data normally provided by tube manufacturers

$$I_D = \frac{\tau}{4(n_f)^2 (1+m)^2} \cdot \frac{a E \tau}{L_e} \cdot \mu \int_0^\infty \epsilon(\lambda) K(\lambda) d\lambda \tag{5}$$

The factor $\int_0^\infty \epsilon(\lambda) K(\lambda)\, d\lambda$ is the combined sensitivity in ampere/watt of the phosphor light source of the storage tube coupled to the dissector photocathode.

To arrive at an estimate of the current output of the dissector the following computations and assumptions are required to utilize Equation (5). For the problem at hand a P-20 phosphor is used by the FW232 image storage tube and an S-20 photocathode is employed for the F4011 dissector tube. This combination yields,

$$K^* = \int_0^\infty \epsilon(\lambda) K(\lambda)\, d\lambda = 38.1 \times 10^{-3} \text{ amperes/watt}$$

A plot of $\epsilon(\lambda) K(\lambda)$ may be found in Figure 20. The aperture diameter corresponding to a 450 x 450 array of elements is $d = \frac{1.1}{\sqrt{2}} \cdot \frac{1}{450} = 1.724 \times 10^{-3}$ inches $= 4.38 \times 10^{-3}$ cm. This yields an aperture area, $a = 1.51 \times 10^{-5}$ cm^2. The luminous efficiency of the P-20 phosphor is $L_e = 480$ lumen/watt. The magnification, m, was computed as 0.733. A 14 stage photomultiplier has been selected which has a typical gain of $\mu = 2.5 \times 10^8$, this assumes the average gain per stage is four. (The standard photomultiplier of the F4011 consists of 10 stages. The higher photomultiplier gain is required to render useful output currents.) The f/number n_f is set equal to unity to minimize light attenuation. The maximum value of E_T is stated by the manufacturer to be 2×10^{-3} lumen/cm^2. This value of $E_{T(max)}$ is attenuated by a factor of 0.75 to insure that the storage tube is operating in a reasonably linear range. This yields a usable E_T of 1.5×10^{-3} lumens/cm^2. When these values are substituted into Equation (5) the resulting output current is calculated as:

$$I_{D_{max}} \cong 26.2 \text{ microamperes.}$$

4.3.3 Number of Gray Levels

The number of detectable levels at the output of the image dissector is dependent upon the magnitude of the noise current of the dissector. The primary source of noise in an image dissector is due to the

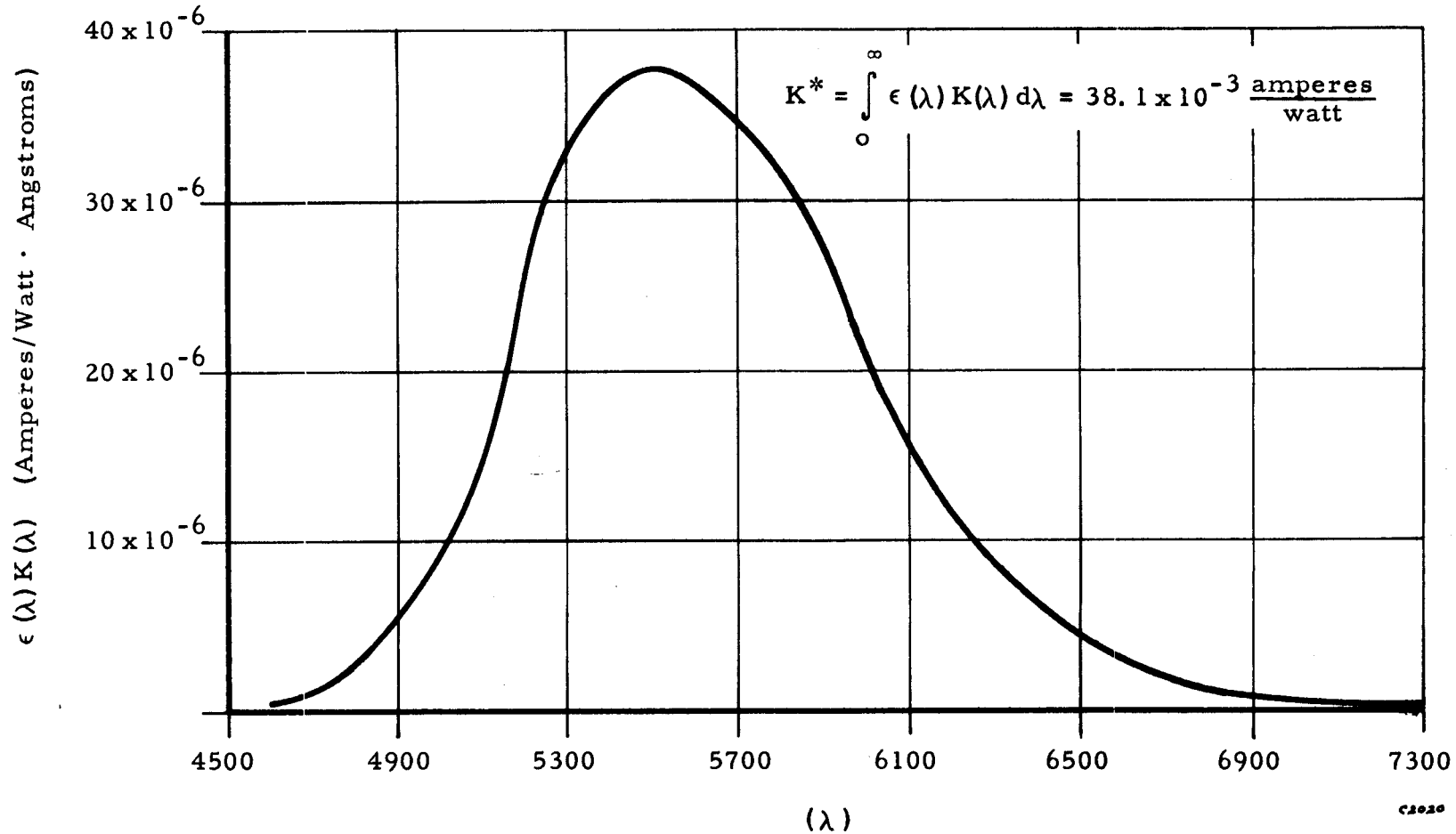

Figure 20. Sensitivity Per Unit Wavelength ($\epsilon(\lambda) K(\lambda)$ for P-20 Phosphor to S-20 Photocathode)

random shot noise present in the photocathode emission. The effect of the photomultiplier is to increase the noise coming through the aperture of the dissector by a factor of 1.15 for the dissector being considered. The well known formula for the output noise current is

$$I_n = \hbar \sqrt{2 e \mu I_D \Delta f} \tag{6}$$

where

$\hbar = \sqrt{\frac{\delta}{\delta - 1}}$, δ = per stage gain of the photomultiplier

e = charge of one electron = 1.6×10^{-19} coulomb

μ = overall gain of the photomultiplier

I_D = average output current of the dissector

Δf = bandwidth of the system.

The useful bandwidth of a system can be no greater than one half the sampling frequency, so that

$$\Delta f = \frac{f_s}{2} = \frac{1}{2 \Delta t}$$

where

f_s = sampling frequency

Δt = time duration between adjacent samples,

so that (6) may be expressed as

$$I_n = \hbar \sqrt{\frac{e \mu I_D}{\Delta t}} \tag{7}$$

This yields

$$\frac{I_D}{I_n} = \frac{\sqrt{I_D \Delta t}}{\hbar \sqrt{e \mu}} = \frac{\sqrt{N}}{\hbar} \tag{8}$$

where

N = electrons collected by the aperture

For the system being considered $\mu = 2.5 \times 10^{8}$ and $\eta = 1.15$, therefore

$$\frac{I_D}{I_n} = \frac{\sqrt{I_D \Delta t}}{7.29 \times 10^{-6}} = 137 \times 10^{+3} \sqrt{I_D \Delta t} \qquad (8')$$

If t_v = maximum allowable viewing time of the image storage tube then it is necessary that

$$\Delta t \leq \frac{t_v}{SM^2}$$

where

S = number of subsections per stored picture frame

M = number of elements in horizontal or vertical direction sampled in each subsection

For the system being considered

S = 121 (50% overlap)

M = 75

t_v = 60 seconds.

The number of samples in a frame is $SM^2 = 680,625$. This gives

$$\Delta t \leq 88.2 \ \mu\text{sec}$$

Using this value of Δt in Equation (8') gives

$$\frac{I_D}{I_n} = 1.29 \times 10^{3} \sqrt{I_D}$$

The number of gray levels N_G, for a fixed current I_D, is approximately

$$N_G = 1 + \frac{I_D}{I_n}$$

These values are given in Table VI. Over the useful current range (0 - 26 μamps) the average number of gray levels obtainable is approximately five.

TABLE VI

NUMBER OF GRAY LEVELS

I_D μ amps	$1 + \frac{I_D}{I_n}$
26	7.58
22	7.05
18	6.47
14	5.83
10	5.08
6	4.16
2	2.82

5.0 PARALLEL/ANALOG RECOGNITION SYSTEM

Two variations of the parallel/analog recognition system were studied. They differ in the technique used to provide information in a parallel format to the recognition device. Each of the system variations utilize the lenses, image storage tube, and image dissector tube discussed in Section 4.2 and shown in Figure 16.

5.1 System I

This system involves a direct view storage tube to convert the electrical output of the dissector tube to a visible image of the subregion being sampled. The storage display tube is coupled via a relay lens to a photosensitive array (Figure 21).

A number of available storage display tubes were studied for system applicability. It was found that in order to mate a 75 x 75 array of discrete photodiodes to a display storage tube, a tube much too large to be considered practical (even if they existed as off-the-shelf items) would be required. One of the smallest discrete photosensors that may be realistically used is the TI LS600. A 75 x 75 array of LS600 silicon photodiodes (0.092 OD) would occupy a square of approximately 7.5 inches on a side. With existing off-the-shelf display storage tubes (with their attendant resolutions) it was found that in order to couple the tube with the 7.5 inch square array a magnifying lens with magnification from 4X to 6X would be required. This would add what is unquestionably a large and impractical linear dimension to this portion of the system.

Since in the present state-of-the-art, useful discrete arrays smaller than a 7.5 inch square format do not exist, monolithic arrays were investigated. In this case, state-of-the-art was such that near-time development of a 50 by 50 element array was highly probable. This was in fact the resolution used on the Lunar experiments. Larger arrays (i.e., containing more elements) should certainly be developed in the near future. The 50 by 50 array will be discussed to demonstrate the feasibility of using this technique to provide parallel inputs to the recognition system.

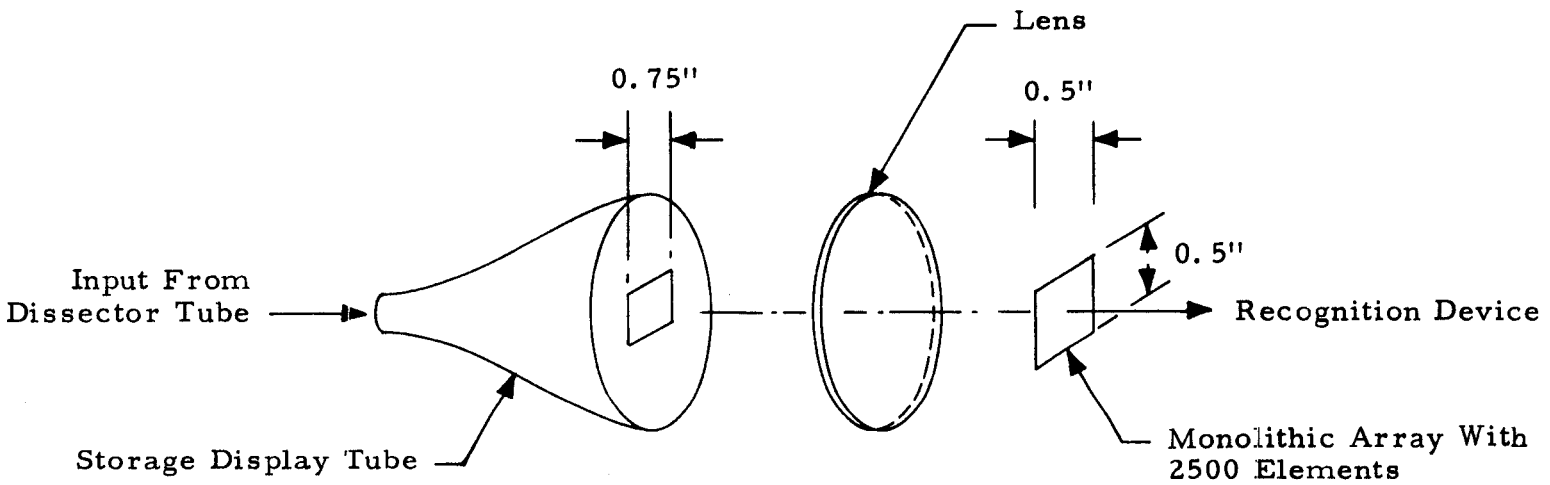

Figure 21. System I

5.1.1 Monolithic Sensory Array

An array is currently under development by the Solid State Electronics Department of Douglas. The unit will consist of 50 x 50 elements. The optical image size of the array is 0.5 inch x 0.5 inch. The unit will be constructed using silicon phototransistors. A unique feature of this array is that it provides 2500 parallel outputs. The problem of separate contacts to each sensor is solved by multilayer metal contact patterns evaporated on the back side of the array. This array is enclosed by a dielectric material which has wires embedded in it. Nine contact layers are evaporated to connect each sensor with one embedded wire. Eight insulating layers are required. This approach makes monolithic arrays applicable for a parallel analong recognition system providing that such arrays may be constructed with sensor uniformity better than 6%. To achieve good uniformity the maximum size of the Si wafer used to fabricate the array is held to 0.707 diameter. This minimizes the radial variations due to crystal nonuniformity. The merits of this approach await laboratory evaluation of the resultant array.

An alternate approach is to construct a monolithic array using thin film techniques (CdS) rather than Si junction devices. This approach should yield devices which have better uniformity and sensitivity than silicon. This approach is being developed concurrently with the Si array.

5.1.2 Display Storage Tubes

This tube could be used to store a scanned subsection and display the subregion image to an array of photo sensors. The input under such conditions is the electrical output of the dissector.

One requirement of this device is that it be capable of writing the subsection image at a rate equal to or greater than the input scanning rate. The writing rate, v, of these tubes is specified in inches/sec. If the number of elements in the horizontal or vertical direction of each subsection to be displayed is M, the display tube resolution designated R, and tube diameter by d, then the writing time t_w is described by,

$$t_w = \frac{M^2}{Rv} \quad \text{if} \quad \frac{M}{R} < \frac{d}{\sqrt{2}}$$

Choosing t_w = 88 usec and M = 75 requires that v = 6.4 x 10^5 inches/sec for the ITT F3015 display storage tube having R = 100 TV lines/inch. The specified writing speed of this tube is 2.5 x 10^5 inches/sec. Increasing the writing speed has the effect of reducing the output luminous emittance by a factor of 6.4/2.5. However, this is not a serious problem since the emittance of the display tube is much larger than required to be detected by the elements of the photo sensor array.

The total time to erase this tube is 10 msec. With 121 subsections this yields a total erasure time per frame of 1.21 seconds (requires storage tube to hold 61.2 sec as opposed to 60 sec). The size of a subsection on the display storage tube is a square having sides M/R = 0.75 inch. A coupling lens is used to image the 0.75 inch x 0.75 inch square onto the array.

The display storage tube, coupling lens, and monolithic array are well matched, i.e., the display tube will provide an output well within the useful range of the photosensors of the array (above dark current and below saturation).

5.2 System II

In this system (see Figure 22) the output of the dissector is sampled and stored in a bank of sample and hold circuits. After all $(75)^2$ samples are stored the sample-hold bank is interrogated to provide the inputs (in parallel format) to the analog recognition device.

5.2.1 Sample and Hold Circuits

The general structure of a sample and hold circuit is shown in Figure 23. The major requirement for the switch S is that it be a high speed switch, having a low "ON" resistance and a high "OFF" resistance and be capable of bilateral current flow. The latter requirement is sometimes deleted at the expense of a shunt dumping switch in parallel with the capacitor, C.

The overall sampling accuracy is dependent on the ratio of the hold time to the sample time for a fixed source and load resistance, and is independent of C.

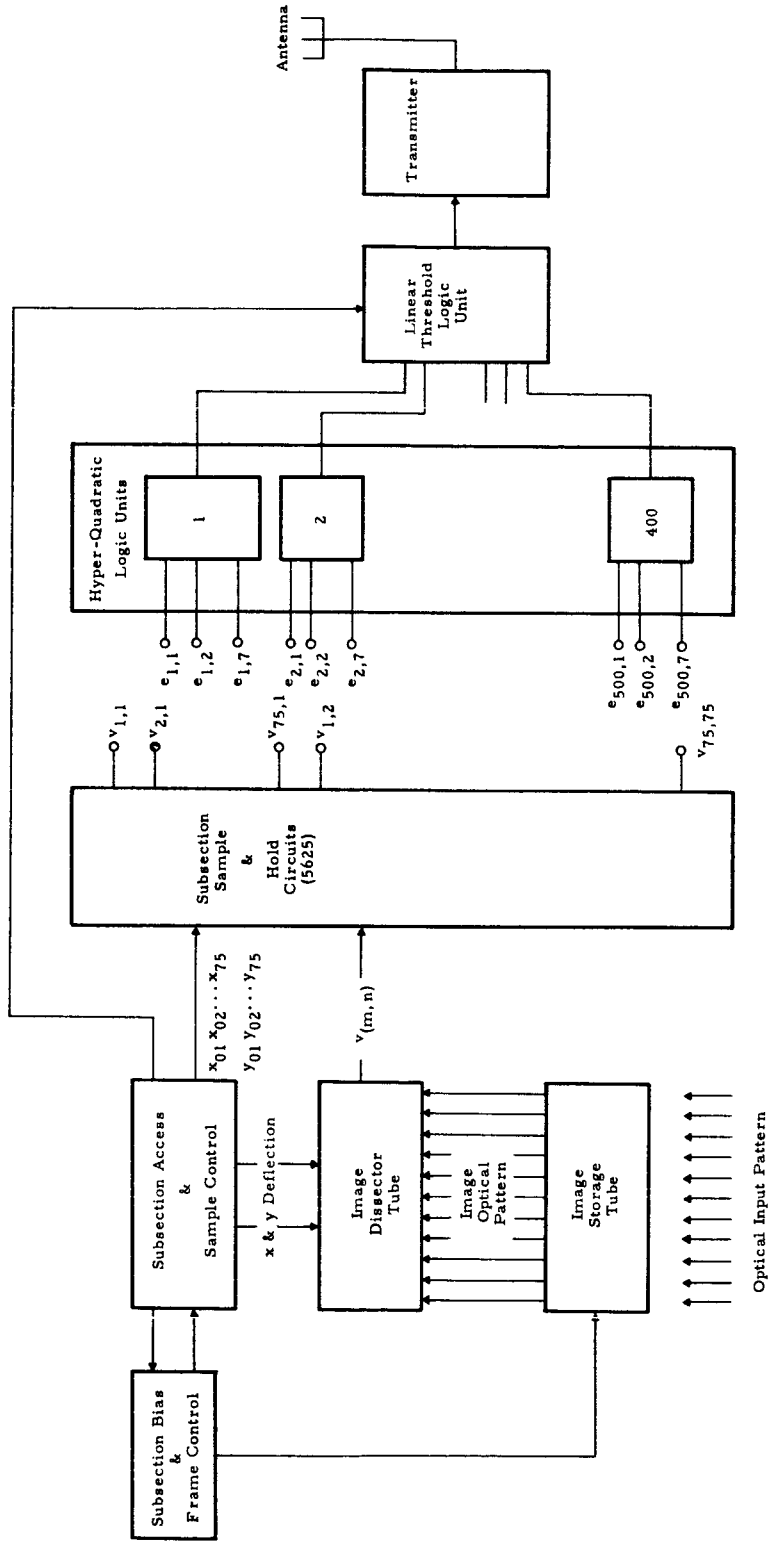

Figure 22. Simplified Block Diagram Parallel/Analog Recognition System (with Capacitive Array)

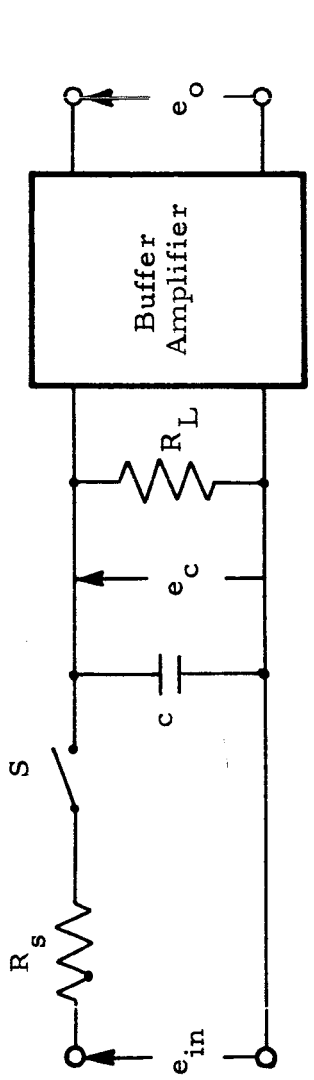

Figure 23. Typical Sample and Hold Arrangement

If

t_S = sampling time = dissector dwell time

t_H = hold time = storage time/number of subsections = 60/121

a = required sampling or hold accuracy

then

$$t_S = R_S C \ln \frac{1}{a}, \text{ and } t_H = R_L C \ln \frac{1}{1-a} \cong R_L C \cdot a$$

so that

$$\frac{t_H}{t_S} = \frac{R_L}{R_S} \cdot \frac{a}{\ln \frac{1}{a}}$$

Consider a system requiring eight uniformly spaced gray levels, that is, a spacing between gray levels of 12.5%. Then it is reasonable to take a = 3% which gives a combined sampling and hold error of 6%. If t_H = 500 msec and t_S = 88 usec then $\frac{R_L}{R_S} = 0.66 \times 10^6$.

A reasonable value for a solid state switch is R_S = 50 this gives $R_L \cong$ 33 megohms. Substituting in the value of R_L gives C $\cong$ 90 picofarads.

By constructing the buffer amplifier in a unity gain configuration and utilizing a matched pair of field effect transistors in the input stage of the amplifier, it is possible to realize input resistances greater than 100 megohms.

The power dissipated by the control gating circuits may be made sufficiently small so as to be neglected relative to the dissipation of the buffer amplifier. The buffer amplifier should be capable of accepting and outputing a zero to ten volt signal. High level signals are conducive to good operation of the first layer logic units which these amplifiers supply. This indicates that it will be difficult to construct a buffer amplifier using less than 5 milliwatts.

5.2.2 Hyper-Quadratic Logic Unit

The performance of each of these first layer logic units is determined by the relation

$$e_o = 1 \quad \text{if}$$

$$\sum_{i=1}^{7}\sum_{j=1}^{7} W_{ij} e_i e_j - \theta = \sum_{i=1}^{7} e_i \sum_{j=1}^{7} E_{ij} e_j - \theta \geq 0$$

and $e_o = 0$ if

$$\sum_{i=1}^{7}\sum_{j=1}^{7} W_{ij} e_i e_j - \theta < 0.$$

Where e_o is the output of the first layer logic units and e_i and e_j are the inputs which originate from the capacitive sampling array or from the photo sensor array.

In expanded form the equation for the hyper-quadratic surface contains 49 terms. Seven of these terms involved squaring the components of each input vector and 42 involved cross-products of the components of the input vectors taken two at a time. If we define

$$u_{ij} = W_{ij} + W_{ji} \qquad i \neq j$$

and

$$u_{ii} = W_{ii}$$

then

$$\sum_{i=1}^{7} e_i \sum_{j=1}^{7} W_{ij} e_j \equiv \sum_{i=1}^{7} u_{ii} e_i^2 + \sum_{i=1}^{6} e_i \sum_{j=i+1}^{7} u_{ij} e_j$$

In expanded form the right hand member of the above equation contains seven square terms and twenty-one cross-products. A block diagram of the minimal structure indicated by the above equation for a seven input logic unit is shown in Figure 24. The structure is minimal in the sense that the number of weighting resistors is minimized as well as the number of connections internal to the logic unit.

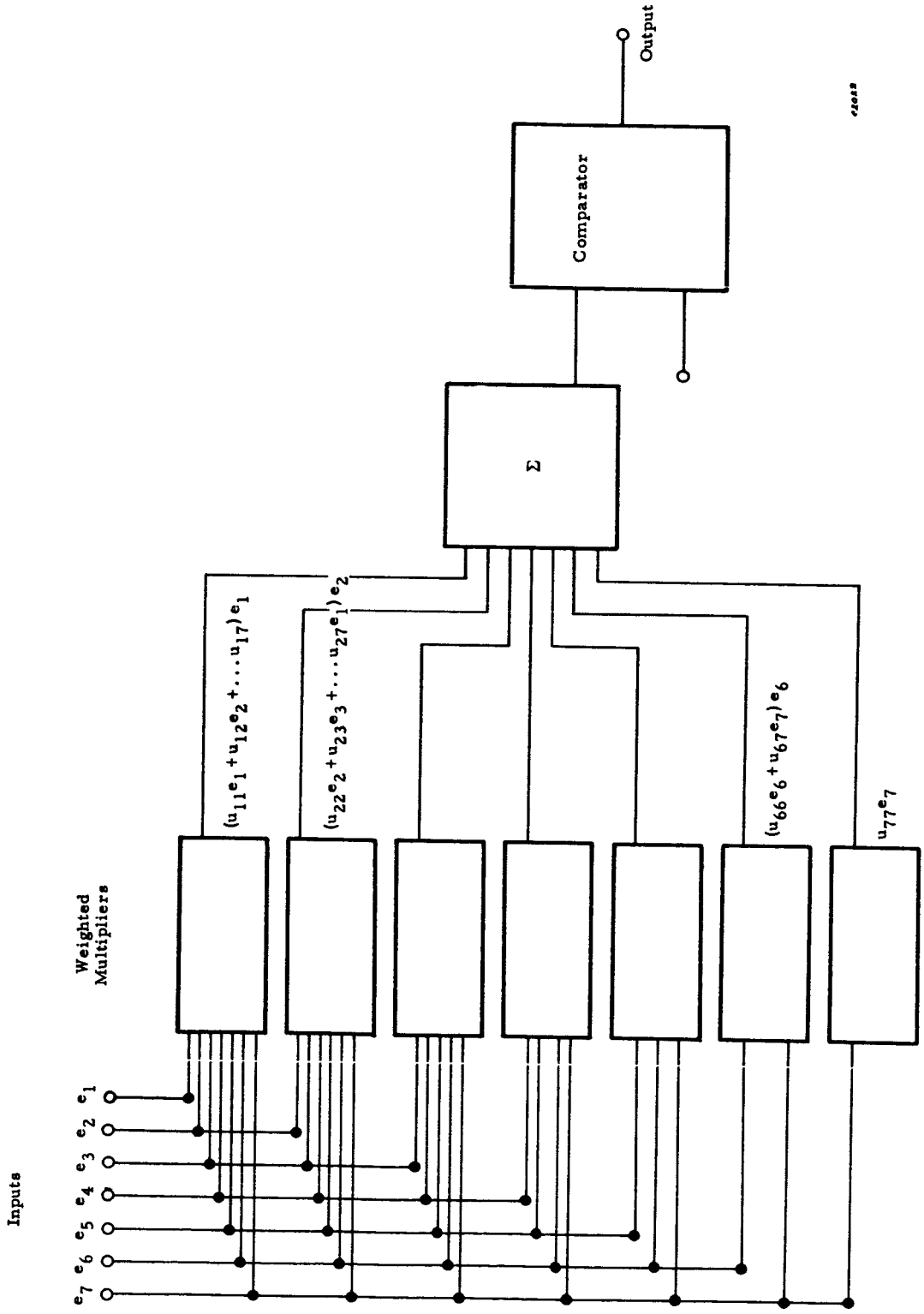

Figure 24. Hyperquadratic Logic Unit Connective Structure

Since many of these hyper-quadratic logic units are required by a useful recognition system it is important to keep the weight and power utilized by each as small as possible. Further, it is important to maintain the response time, t_R, of each unit as small as possible in order to obtain the high data processing rates normally associated with a parallel analog recognition system. The servo multiplier technique using ganged potentiometers operates accurately but has the disadvantages of large weight and size and a poor frequency response. The disadvantage of utilizing the Hall generator technique[2] is its weight and the power required to obtain a useful output. For example, a Hall multiplier using conventional toroidal magnets for a seven input quadratic logic unit will weigh approximately 3.5 pounds. For a system requiring approximately 400 quadratic units a weight of 0.7 tons would be involved.

A method which overcomes the disadvantages of servo-multipliers and Hall multipliers is to utilize the logarithmic relationship between the transistor emitter current and the base to emitter voltage. This relationship is extremely uniform from transistor to transistor if the devices currently used for differential amplifier applications are employed. Figure 25 is a plot of V_{BE} vs. i_e for 1/2 of an MD1122. The graph was obtained from measurements on 5 differential transistors (10 functions). The variation of the base to emitter voltage for any emitter current from 2 μa to 100 μa is less than $\pm .200$ volts. This variation will cause a maximum absolute error over the current range from 1 μa to 1000 μa of less than $\pm 5\%$.

The operation of the weighted multipliers used for the quadratic logic unit is described with the aid of Figure 26. Each weighted multiplier used by this logic unit is identical in its principles of operation. Initially v_x, v_y and v_B are shorted and the off-set pot adjusted so that $v_{BE} = 0$. This accounts for any D.C. offset appearing across the input terminals of the μa 709 integrated circuit amplifier. In an actual system, where size and weight are important the offset pot may be replaced by two fixed resistors.

The μa 709 amplifier is connected as a differential amplifier so that

$$v_{BE} = v_x + v_y - v_B$$

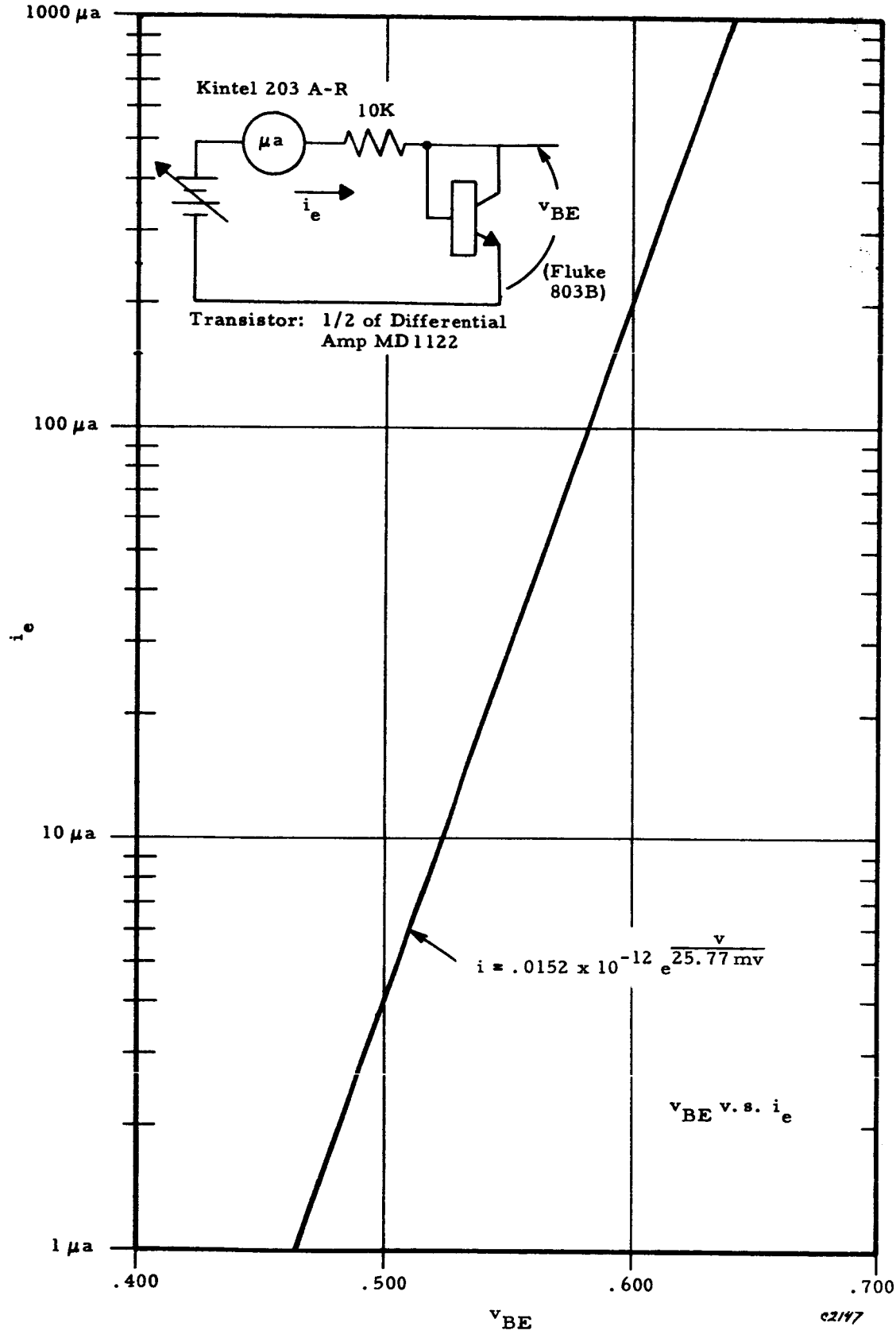

Figure 25. Plot of Emitter Current vs. Base to Emitter Voltage

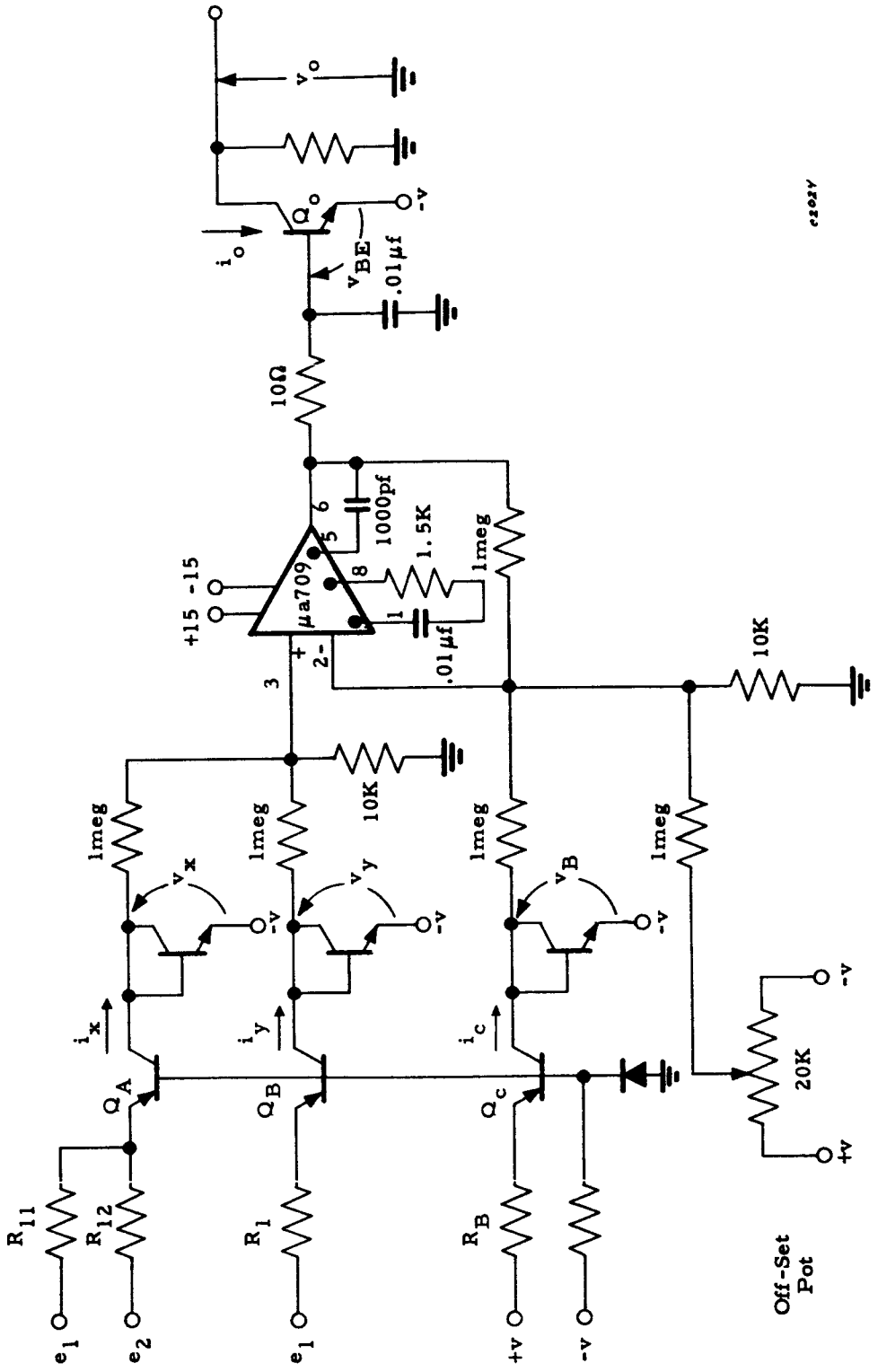

Figure 26. Weighted Multiplier Schematic

This expression may be rewritten using the semilogarithmic relations between voltage and current to yield

$$\frac{KT}{q} \ln \frac{\alpha_o i_o}{i_R} = \frac{KT}{q} \ln \frac{i_x}{i_R} + \frac{KT}{q} \ln \frac{i_y}{i_R} - \frac{KT}{q} \ln \frac{i_c}{i_R}$$

or

$$i_o = \alpha_o \frac{i_x i_y}{i_c}$$

but

$$i_x = \alpha_a \left(\frac{e_1}{R_{11}} + \frac{e_2}{R_{12}} \right)$$

$$i_y = \alpha_B \frac{e_1}{R_1} ; \qquad i_c = \alpha_c \frac{v}{R_B}$$

and

$$v_o = -i_o R_L = -\alpha_o \frac{i_x i_y}{i_c} R_L$$

hence the output voltage is given by

$$v_o = -e_1 \left(\frac{\alpha_a \alpha_B \alpha_o}{\alpha_c} \right) \left(\frac{R_B R_L e_1}{R_{11} R_1 v} + \frac{R_B R_L e_2}{R_{12} R_1 \cdot v} \right)$$

If Q_a, Q_B, Q_c, and Q_o are high beta transistors having a $\beta_{min} = 100$ and a $\beta_{max} = 200$

then

$$.98 < \frac{\alpha_a \alpha_B \alpha_o}{\alpha_c} < .99$$

so that,

$$v_o \cong -v_x \left(\frac{R_B R_L}{R_{11} R_1} \frac{v_x}{v} + \frac{R_B R_L}{R_{12} R_1} \frac{v_y}{v} \right)$$

by equating like terms it is apparent that

$$u_{ii} = \frac{R_B R_L}{R_{ii} R_1} \frac{1}{v} \quad \text{and} \quad u_{ij} = \frac{R_B R_L}{R_{ij} R_1} \cdot \frac{1}{v}$$

In constructing this weighted multiplier it has been assumed that the $i_{Rx} = i_{Ry} = i_{RC} = i_{Ro}$. This condition can be met only if the transistors are mounted on a common heat sink or even to a higher degree if they are mounted on a common header. That is, a unit containing matched transistors mounted on a single TO-5 header.

To allow summing of the individual products, see Figure 27, it is only necessary to mutually connect the output collectors of all the individual weighted multipliers and terminate these collectors in the common load resistor R_L.

The output comparator may be readily constructed using an integrated circuit μa 710 which is housed in a TO-5 case.

The total components used for a quadratic logic unit are tabulated below in terms of the number of inputs/logic unit, n (Table VII).

A seven input logic unit would require a volume of less than 2 cubic inches and weight approximately 0.1 pound. The power dissipated by each logic unit using the conventional components listed above is approximate (80 milliwatts)(n). For n = 7 the dissipation is 0.56 watts. Future integrated circuit amplifiers could afford significant reduction in this power dissipation.

5.2.3 Single Hyperplane or Linear Threshold Unit

The response layer is constructed with linear threshold logic units (Figure 25). The equation defining the performance of these units is

$$\sum_{i=1}^{n} w_i e_i > \theta$$

$$w_i = \frac{R_p}{R_i} \quad \text{where} \quad R_p = \frac{1}{\frac{1}{R_1} + \frac{1}{R_2} + \frac{1}{R_3} + \ldots \frac{1}{R_n}}$$

TABLE VII

COMPONENTS OF QUADRATIC LOGIC UNIT

Component Type	Quantity as a Function No. of Inputs	With n = 7
Resistors	$\frac{(n)\ (n+1)}{2} + 11n + 3$	108
Capacitors	$3n + 4$	25
Matched Transistors (4/T0-5 Case)	n	7
Differential Amps (μa 709 integrated)	n	7
Comparator Amp (μa 710 integrated)	1	1

The allowable differential input voltage is ±5 volts.

$$e_o \cong o \quad \text{if} \quad \sum_{i=1}^{n} w_i e_i < \theta - (5 \text{ mv})$$

$$e_o \cong +3 \quad \text{if} \quad \sum_{i=1}^{n} w_i e_i < \theta + (5 \text{ mv})$$

Optimum sensitivity and minimum drift are obtained by using small values of R_p; however, such optimization is not a necessary system requirement. A reasonable range for R_p would be from 5 to 50KΩ.

Figure 27 is a schematic diagram of an integrated circuit differential amplifier which is used in constructing the linear threshold unit. Figure 28 is a diagram of a typical linear threshold unit with positive weights. Negative weights are achieved by inputting the selected e_i's to the opposite side labeled 3 in Figure 28.

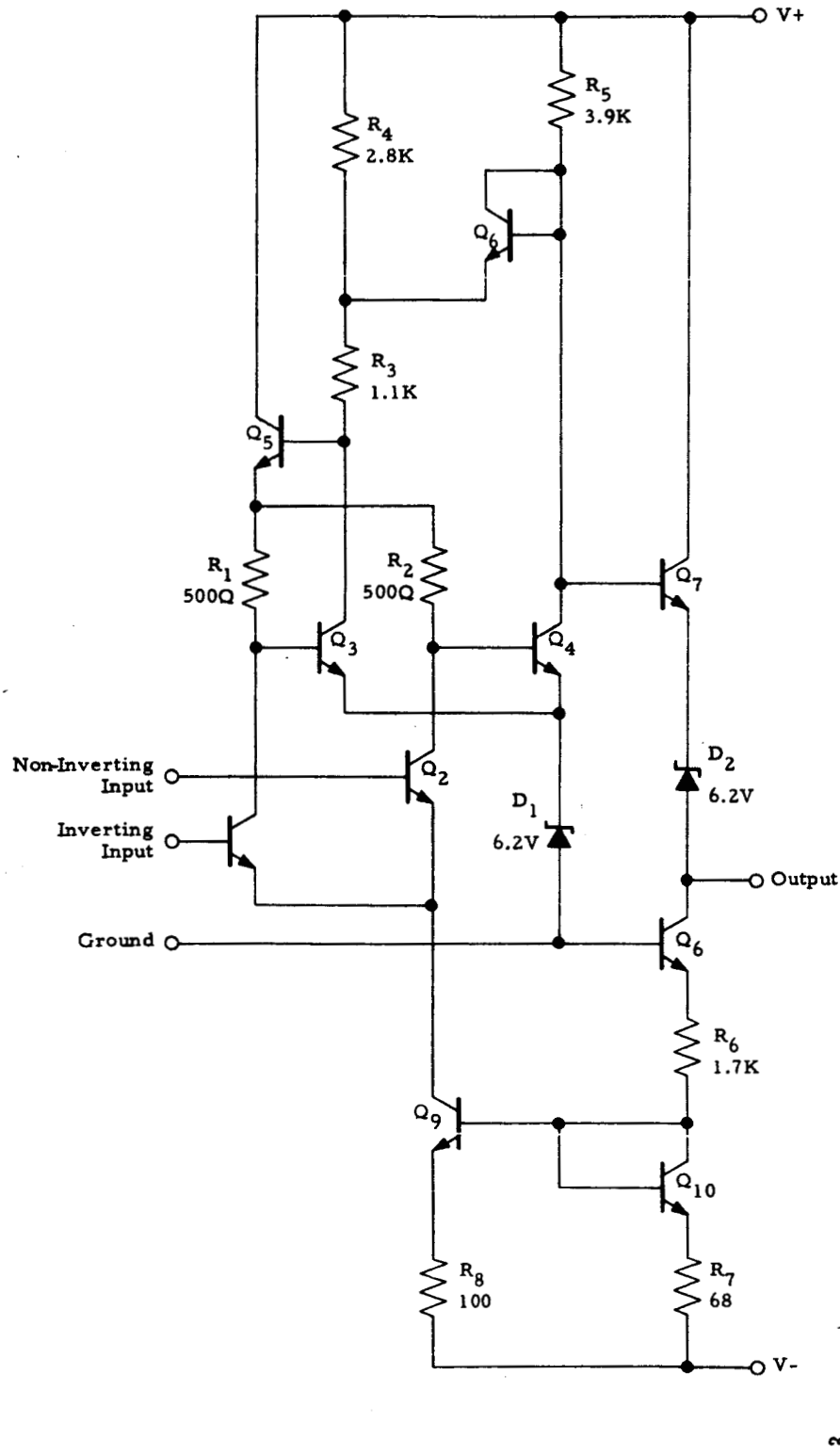

Figure 27. μa 710 Integrated Circuit Differential Voltage Comparator

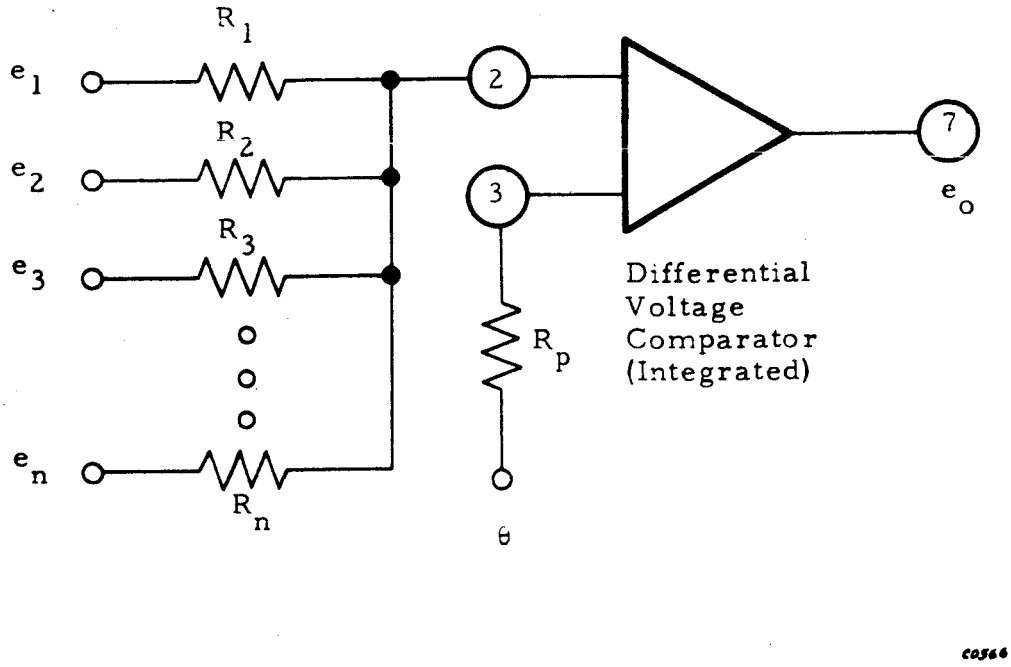

Figure 28. Linear Threshold Logic Unit (I. C.)

5.3 Summary of the Results of the Feasibility Study

Both of the systems studied appear to be feasible although there are problem areas which require further study before a final assessment of feasibility is made.

For the recognition problem considered the combination of image storage tube and image dissector tube provides adequate resolution. If the requirement that the input to the recognition device be obtained from an array containing $(75)^2$ samples is retained, a decrease in the size of the subregion which provides sample inputs would increase the resolution requirements for the image storage tube. It is not likely that much finer storage meshes will be available in the near future so that greater resolution for the image storage tube can best be obtained by constructing a larger diameter tube. For the image dissector tube resolution is not a limiting factor since the resolution at which it will operate is determined by the size of the sampling array. The limiting resolution of the dissector tube in any event far exceeds the needs for the classification problem under consideration.

The maximum output of the image dissector tube for the NIMBUS space environment has been calculated to be 26 μ amps. Within this range the average number of distinguishable current levels (associated with distinguishable gray levels in the system input image) has been calculated to be five. The number of output gray levels can be increased by obtaining a higher current at the aperture of the dissector tube. Since the area of the aperture is fixed this can only be accomplished by increasing the output brightness of the image storage tube. Techniques exist for doing this – at the expense of a slight increase in system complexity.

In System I the parallel inputs to the recognition device were obtained through the use of a display storage tube for imaging a subregion scanned by the dissector, a relay lens, and a monolithic array of 50 x 50 element format. The array is not an off-the-shelf item but it and larger arrays are currently under development.

In System II, which involves a bank of sample-hold circuits as a means of supplying the parallel format to the recognition device, the design of the sample-hold circuits is dependent upon the ratio of the storage tube hold time

(total processing time) to the single element dwell time of the dissector tube. Specifically, for the present problem, the input resistance for the buffer amplifier coupling the sampling capacitors to the logic units must be approximately 33 megohms. The design of these circuits thus requires up to date state-of-the-art techniques but are realizable.

Practical, lightweight, analog quadratic logic units are currently not available. However, a very promising circuit design using matched transistors and integrated circuit differential amplifiers has been breadboarded and evaluated and appears to satisfy the requirements. The weight of such a unit would be approximately 0.1 pound.

The total number of bits which must be transmitted in order to reconstruct the image stored in the image storage tube is $3 \cdot (540)^2 = 7.75 \times 10^5$ bits. Transmitting only the classification of each of 121 subregions (into one of four possible classes) requires 242 bits. This represents an improvement of 3200 to 1 in total bits transmitted. The ratio is so high that it makes little sense to consider the ratio of power required to transmit the entire picture to that of transmitting only the classification of 121 subsections.

The physical dimensions (weight and size) and power required are approximately those give in Table VIII. Although the power required for the operation of the recognition systems are high compared to existing satellite systems it should be remembered that (for the most part) off-the-shelf items were used. It is probable that a reduction in power of four or five to one may be possible with the development of a sequential/digital realization of a recognition system using the image storage tube in the preprocessor without sacrifice in the processing time.

TABLE VIII

PHYSICAL DIMENSIONS AND POWER

Component	Weight (pounds)	Size	Power (watts)
Image Storage Tube	8	5.75" x 5" OD	1.2
Image Dissector Tube	3.5	6.5" x 3.1" OD	1.2
Lenses			
Input	1		
Errector	4		
Total for Image and Dissector Tube Sub-System	16.5	25.5" x 5" OD	2.4
Sample-Hold Bank	70	6" x 10" x 17.5"	28
Photosensitive Array	3	45" x 6" OD	70
Recognition Device	40	10" x 10" x 10"	200

SYSTEM TOTALS

System I	69.5	12" x 45" x 12"	277.5
System II	126.5	10" x 32" x 10"	234.4

6.0 PROGRAM FOR THE NEXT PERIOD

During the next reporting period the primary effort will be centered on improving the performance obtained on four of the five lunar and NIMBUS tasks. The methods to be used will include a careful screening of the sample patterns to insure that all patterns are positively identifiable by a human observer, the use of subarea scanning, and the use of idealized training patterns. Decision functions will be designed adaptively for the known properties developed by NASA for the NIMBUS patterns. Known properties will be developed for lunar patterns. The known property sets will be augmented by statistically derived properties designed to complement them, and the combined sets tested to evaluate this important process.

A program to implement a cluster analysis will be written, to evaluate this analysis as a possibly improved method for the design of property filters or decision functions. Improvements to the adaptive algorithms already under evaluation, particularly the MADALINE technique, will be sought.

The study to determine the feasibility of an on-board recognition system will be continued. Specifically, a sequential/digital system will be investigated. This system will utilize the sequential output of the dissector tube (or perhaps a vidicon) as inputs to a special digital computer realization of a recognition device. If feasible, such a system could achieve a significant reduction in weight and power required over the systems already studied.

Consideration will also be given to a system in which the storage tube is replaced by an electromechanically driven mirror system to display a subsection on a photosensitive array or on the face of a scanning tube.

Refinement of the quadratic surface logic unit will be attempted and trade-offs made in the various elements of the parallel/analog recognition systems to achieve a system consistent with the requirements for satellite instrumentation and with the results of the recognition experiments being conducted.

REFERENCES

1. American Institute of Physics Handbook, pp. 2 - 241.

2. Design of a Cloud Pattern Recognition System, Final Report on Contract NAS 5-3866, Astropower Laboratory Report SM-46215-F, October 1965.

CORRIGENDA

In the lunar feature experiments reported in Technical Progress Report No. 2, a bug was detected in the "error correction" programs. The computer program which designs the linear decision function records the final design on magnetic tape. A second program then reads the decision function from the tape and determines the performance of the system on the generalization patterns. For the "error correction" technique only, the threshold was not being stored in the proper location prior to being recorded on tape. The net result was that the generalization performance was tested against an essentially random threshold.

The correct values for the thresholds were determined from the printout and force-fed into the generalization testing program. The resulting performance levels were determined, and the corrected data are presented in Figures C17, C20, and C23. As in the last report, two thresholds are considered for "error correction." One threshold is computed as part of the adaptive routine, and the second at the end of the routine. The latter threshold is the average value of the linear decision function for all of the training patterns. Data for the latter threshold appears in the second line. With the corrected values, the "error correction" procedure gives performances equal to the best technique, "iterative design," on the lunar data.

It is again noted, that Figures C17, C20, and C23 differ from the corresponding Figures 17, 20, and 23 of TPR-2 only in the generalization performance for the "error correction" technique.

Technique	% Design Pats.		% Gen. Pats.		Best % Gen. Pats.	
	SDA	DAID	SDA	DAID	SDA	DAID
Forced L.	65.45	82.60	51.00	62.75	62.50	63.75
Bayes W.	65.60	84.10	51.00	63.75	62.50	65.50
Error Corr.	87.05	92.80	55.75	59.75	61.00	61.50
	87.10	92.85	54.50	59.75		
Iter. Des.	89.80	92.10	55.00	59.00	59.50	61.50
Mean Sq.Er.	57.35	81.80	52.00	53.00	57.25	56.00
Madaline	72.20	100.00	54.00	58.00		

Figure C17. Craters With Central Elevations vs. Craters Without

Technique	% Design Pats.		% Gen. Pats.		Best % Gen. Pats.	
	SDA	DAID	SDA	DAID	SDA	DAID
Forced L.	70.40	81.20	72.25	71.0	75.25	74.25
Bayes W.	70.40	82.60	72.50	75.25	75.25	78.50
Error Corr.	90.25	83.45	65.50	51.0	67.00	74.25
	92.00	100.00	65.00	70.25		
Iter. Des.	92.10	100.00	64.00	73.75	65.75	76.00
Mean Sq.Er.	78.55	91.35	56.25	74.50	57.50	76.50
Madaline	80.30	95.80	67.50	75.75		

c18/9

Figure C20. Rima vs. Wrinkle Ridges

Technique	% Design Pats.		% Gen. Pats.		Best % Gen. Pats.	
	SDA	DAID	SDA	DAID	SDA	DAID
Forced L.	76.55	78.50	77.50	74.75	78.25	79.25
Bayes W.	76.55	82.60	77.50	77.50	78.50	84.00
Error Corr.	91.75	94.80	74.00	92.75	75.00	99.25
	97.10	99.20	74.50	99.25		
Iter. Des.	97.25	99.50	74.75	99.50	75.25	99.75
Mean Sq.Er.	91.20	83.25	73.00	82.25	73.50	85.50
Madaline	87.40	87.35	78.25	84.25		

c/822

Figure C23. Craters vs. Linear Features